A molecular dynamics study of ion beam assisted deposition of thin molybdenum films and analysis by thermal desorption spectrometry

Peter Klaver

supervisors:
dr. Barend J. Thijsse
ir. Leon D. van Ee

Delft University of Technology
Faculty of Applied Sciences
Materials Science Department
FCM-1

april 1998

Contents

Summary 4
1 Introduction 7
2 Molecular dynamics 10
2.1 General principles 10
2.2 Interaction potentials 10
2.3 Implementation on a computer 16
2.3.1 The system in a box 16
2.3.2 Numerical algorithm 18
2.3.3 Timestep control 18
2.3.4 Accuracy, numerical stability, and reproducibility 22
2.3.5 Box size, heat conductance, and simulation timescale 23
3 Scope of the simulations 24
4 Results 26
4.1 Verification and accuracy tests 26
4.2 Surface relaxation 26
4.3 Depositing films 29
4.3.1 PVD films 29
4.3.2 Influence of argon ions on vacancies and surface roughness 33
4.3.3 Influence of the deposition angle on vacancies and surface roughness 38
4.3.4 Influence of the deposition rate and temperature 41
4.3.5 Surface roughness explained by activation energies 42
4.4 Helium decoration 44
4.5 Annealing films 50
4.5.1 Surface diffusion 50
4.5.2 Bulk diffusion 54
5 Conclusions & recommendations 56
Acknowledgements 58
Literature 59
Appendix A 60

Summary

In this thesis classical Molecular Dynamics (MD) simulations are calculated by solving Newtons equations of motion for a system consisting of atoms already condensed onto a substrate and various amounts of impinging atoms and ions. The results of these simulations are lists of the positions and velocities of the atoms. From these positions and velocities various sorts of information about the system of atoms can be determined.

Potentials have been used, and partly adapted, to model interactions between molybdenum, argon and helium atoms. At distances larger than 2.08 Ä the Mo-Mo interaction is modelled by the Johnson-Oh EAM potential. At distances shorter than 1.59 Å this interaction is modelled by the Firsov-Molière Screened Coulomb potential. The Screened Coulomb potential is also used to model all noble gas interactions. The Velocity-Verlet algorithm with a specially constructed variable timestep technique is used to numerically solve Newtons equations.

The algorithm and potentials are part of the MD program Camelion. This program has been used to perform simulations of the deposition of molybdenum films on molybdenum substrates (sometimes assisted by an argon ion beam) the decoration of deposited films with helium ions for Thermal helium Desorption Spectrometry (TDS), and the annealing of films. These simulations are performed as a complementary technique to experimental work. Systems of up to 12000 atoms have been simulated for up to 11 ns. The short simulation times enforce a deposition rate of 0.5 m/s, a rate $5*10^9$ times higher than the experimental rate of 1 Å/s.

Simulations of the deposition of films without ion assistance (PVD) show that, apart from the inclusion of vacancies and large vacancy clusters, (100) films remain almost flat during deposition, whereas (110) films develop columns. The inclusion of vacancies and large vacancy clusters and the lack of columns on (100) surfaces is explained by the reconnection of protruding edges around unoccupied lattice sites. Protrusions attract slightly more atoms than depressions and grow during deposition. As a result of this the unoccupied lattice positions below these protrusions become sealed off from the incoming molybdenum atoms. The edges of the protrusions reconnect, incorporating the unoccupied sites as vacancies. After a cluster of vacancies has been sealed off, the surface is almost flat again. The (110) surface evolves differently. Small protrusions appear as on the (100) surface, but these do not reconnect and continue growing, resulting in a columnar structure. Thick (110) films contain fewer defects than (100) films because unoccupied lattice sites are incorporated into grain boundaries instead of forming vacancies and clusters as in (100) films. However, both (100) and (110) PVD films contain far more defects than found under experimental growth conditions. This is a result of the high deposition rate. During the simulations there is no time for the diffusion that takes place in real experiments. Therefore, in simulations surface vacancies are often left open and turn into bulk vacancies, while in experiments these surface vacancies are often filled by diffusion. The experimental defect concentration of PVD films on of the order of 10^{-4}, while in simulations (100) films have a defect concentration of about 1 percent and (110) films have a defect concentration of about 0.5 percent in the first 30 Å of deposition, and 0.3 percent in the second 30 Å of deposition. The lack of time for diffusion also means that the surfaces of deposited films contain many low-coordinated atoms, most of which would have moved to more stable positions in a real experiment, and that the surfaces are slightly too rough. Even though the roughness of simulated films is slightly too high, it became clear that surfaces of deposited films can be very complex. Local surface geometries become even more complex by surface relaxation, which can easily change the distances between neighbouring atoms by 10 percent compared to bulk values. This means that hardly any two atoms on a surface are in exactly the same position, and that diffusion on such a surface is governed by a wide spectrum of activation energies, rather than just a handful.

Films deposited with ion assistance (IBAD films) differ distinctly from PVD films. Their surfaces are smoother because the energy of the ions enhances diffusion. In simulations the enhanced diffusion also results in a lower defect concentration, $1.5*10^{-3}$ for (110) films grown with 100 eV ion assistance and an ion to atom ratio of 0.2. It should be

noted that in experiments the defect concentration in IBAD films has been found to increase compared to PVD films, because argon ions also create vacancies and vacancy clusters, and real deposited PVD films contain hardly any defects that the argon ions could suppress. In simulations the defect-reducing influence dominates over the creation of extra defects. The defect concentration of simulated IBAD films is in agreement with experimental values.

The events after ion impacts can be studied in detail at the atomic level. Argon ions are either deflected or penetrate through the first few atomic planes, hardly ever past the fifth atomic plane. Atoms that penetrate have a high probability of getting trapped, usually at sites previously occupied by molybdenum atoms. The molybdenum atoms are removed through replacement collision sequences that lead to the surface or end as self-interstitials. An argon atom trapped in a substitutional position increases the distance between the neighbouring molybdenum atoms by 1 percent. In addition to replacement collision sequences, the ions can also transfer their energy to the lattice by local melting and sputtering. The average coordination number of the molybdenum atoms that are displaced by argon ions increases by 0.9, showing the flattening effect of the ion bombardment. As expected, the average values of the numbers of displaced molybdenum atoms, trapped ions, sputtered molybdenum atoms, self-interstitials created, and vacancies created by an impact increase from zero for 25 eV ions to higher values for 100 and 250 eV ions. In one simulation the clustering of separate interstitials into a small interstitial plane was observed.

Apart from the surface orientation and IBAD conditions, other deposition parameters have been investigated, viz. the deposition angle, deposition rate, and film temperature during deposition. Most films were deposited with a 15° off-normal angle. (110) films deposited in this way may exhibit a wave-like pattern, with the wave crests lying perpendicular to the in-plane component of the direction along which the molybdenum atoms impinge. This is a shadowing effect. This is confirmed by the observation that normally deposited (110) films do not show a wave-like pattern but more or less rounded columns. In the direction perpendicular to the film the roughness is not strongly affected by the deposition angle. Since (100) films remain almost flat during deposition, the deposition angle has little effect on the shape of (100) surfaces. However, the defect structure is significantly affected. For some unexplained reason, the defect concentrations in films deposited with a normal and 30° off-normal angle of incidence are much higher (over 2 percent) than that in films with a 15° off-normal angle of incidence. Also, the films deposited with normal and 30° off-normal angles of incidence contain very large vacancy clusters, consisting of a few dozen vacancies. In real experiments these clusters are significantly smaller, but that does not explain the difference between films deposited with different deposition angles.

Altering the deposition rate in simulations a little has no influence. For instance, simulating at twice the usual deposition rate still allows less than 1 percent of the diffusion that would have taken place during experimental deposition.

Increasing the film temperature has the same effect as lowering the deposition rate. The exact factor by which increasing the temperature increases the number of diffusion steps depends on the activation energy for diffusion, but diffusion increases at least by several orders of magnitude if the film temperature is increased from room temperature to, for instance, 2000 K. Depositing a film at 2000 K clearly reduces the vacancy concentration and the number of low-coordinated atoms compared to deposition at 300 K. The surface roughness is also reduced, but only slightly, showing that the presence of columns is not, or only partly, the result of the high deposition rate.

During decoration of films with helium, 70 percent of all helium ions were either deflected from the surface or left the film after temporarily penetrating it. Helium atoms that pass the first atomic plane penetrate 8 Å into the film on average, with strong scattering. The helium atoms that do not leave the film remain trapped mostly in interstitial positions but some in existing defects. In real experiments the interstitially trapped helium atoms have enough time to desorb from the lattice, because they are mobile at room temperature. If films containing helium are heated to 2000 K, the helium atoms become mobile even during the short simulation time. They can get trapped in existing vacancies. During annealing it has also been observed that helium attracts a nearby vacancy by ‘pushing’ the 1 to 3 molybdenum atoms between itself and a nearby vacancy towards the vacancy, effectively

moving the vacancy toward itself, after which the helium atom is trapped in the vacancy. Through this mechanism vacancies can also be split from clusters and can even be pulled in from the surface, creating vacancies near the surface. This is a possible explanation of the surface defects found from (110) TDS spectra. It should be noted that this mechanism has only been observed at high temperature, at which thermal vibrations of the lattice may possibly assist in the motion of the molybdenum atoms. Once helium is trapped in a vacancy, it is immobile for the rest of the simulation, even at 2000 K. Desorption was never observed. One explanation for this is that all helium is trapped below the surface during annealing because of the extra kinetic energy available for molybdenum displacement at high temperature. However, this does not explain why in simulations helium is trapped near the surface in both (100) and (110) films, while in experiments only (110) films show surface defects. It is also possible that the apparent contradiction does not lie in the helium interactions, but in the Mo-Mo interaction near the surface. This suspicion is strengthened by the observation that surface relaxation results are not always in agreement with experimental results or results from other simulations.

A number of films have been annealed at 1500 or 2000 K for up to 12 ns. During annealing a rapid decrease in the number of low-coordinated atoms (atoms with low activation energies for migration) and potential energy was observed. After a few ns the number of low-coordinated atoms reaches an almost constant level. These low-coordinated atoms are responsible for almost all diffusion on the surface. After most of the low-coordinated atoms have found higher-coordinated positions, the average potential energy and the total displacement of all atoms per time interval reach an almost constant level, corresponding to equilibrium surface diffusion. The overall shape of films does not change significantly during annealing. This confirms that the presence of columns is realistic: only low-ccordinated atoms are mobile and during deposition there is no clear trend in the number of low-coordinated atoms, so their behaviour is not very important for the onset of columns.

There is little diffusion activity below the surface during annealing, but a number of observation can be made. The activation energy for vacancy migration, as determined with help of a very simple model, has a value between 0.7 and 1.0 eV, lower than values reported by others. Vacancy clusters consisting of vacancies in next-nearest neighbour positions and elongated clusters tend to become more compact. Self-interstitials are very mobile at 1500 K, much more so than helium interstitials. All separate interstitials disappear in a few tenth of a ns. The small interstitial plane, however, did not disappear, nor did it lose any self-interstitials.

1 Introduction

The properties of thin films form an interesting field of research. From a scientific point of view thin films are interesting because of the different behaviour of atoms near a surface compared to the behaviour of atoms in the bulk of a material. From technological and economic points of view they are important because covering a low-quality material with a thin film of high-quality or special purpose material sometimes enables the use of the (often cheaper) low-quality material in demanding applications. Thin films are also important in the production of devices consisting of many small parts of different materials, such as CPUs, memory chips, and various magnetic and optical devices. The production of some devices does not allow for long heating. For example, multilayers may suffer from interdiffusion if they are kept at elevated temperatures for extended periods and some polycrystalline materials show undesirable grain coarsening. But heating is often used to decrease the number of defects that originate in a film during the deposition process. Ion Beam Assisted Deposition (IBAD) is a technique used to deposit films at a high substrate surface temperature without heating the entire substrate. The purpose of IBAD is to combine the defect-reducing influence of high temperature without the interdiffusion and coarsening side effects. This is achieved by depositing material and simultaneously bombarding the surface with ions, usually argon. The energy of the ions* is insufficient to heat the entire substrate (if it is thick enough), but it is sufficient to heat a thin surface layer. The high temperature at the surface enhances diffusion and this results in a flatter film with fewer defects, because atoms have more chance to reach holes in the surface or find other, more stable potential energy minima. Also, the unidirectional momentum transfer tends to break down protrusions, moving their atoms into other unoccupied lattice positions and flattening the film.

A very sensitive way to study defects in the surface region of a film is Thermal Desorption Spectrometry (TDS). A TDS spectrum is obtained by first decorating a film with small, chemically inert atoms. Helium, approaching the surface as accelerated ions, is the usual choice. These helium atoms experience repulsive forces from the surrounding atoms once they are have been injected into the lattice. Some helium atoms attach to vacancies, vacancy clusters, and other defects because there they are not as strongly repulsed. In effect there is a local potential energy minimum. After decoration the film is heated. At sufficiently high temperatures the helium detaches from the defects by thermal vibrations. This happens when the thermal energy of the trapped helium atoms becomes high enough to overcome the energy barrier that prevents helium atoms from moving away from the defects. Helium detaches from different defects at different temperatures. For instance, helium will detach from a monovacancy in molybdenum at lower temperatures (900-1200 K) than from a vacancy cluster (>1350 K) because helium in a monovacancy is already more tightly ‘squeezed’ by the surrounding atoms, so less thermal energy is required to move it into an interstitial position, where it becomes mobile and can diffuse out of the film. By measuring the desorption flux from the specimen, information is obtained about the types and numbers of defects present in the film. The temperature at which a desorption peak appears provides information about the type of defect, and the area of the peak provides information about the concentration of such defects. In this way the effects of IBAD on the defect structure can be studied by TDS. It is also possible to obtain desorption spectra from argon trapped in the film during the bombardment.

The above mentioned experiments, performed on molybdenum films grown with argon ion assistance are part of the research of section FCM-1 of the of Materials Science Department of Delft University of Technology. The work in this thesis consists of Molecular Dynamics (MD) simulations on the same subject. Such calculations are performed because experimental work and MD calculations form a useful complementary combination. The experimental work provides phenomenological information in the form of a desorption spectrum, but it can be difficult, sometimes even impossible, to draw atomic level conclusions from a spectrum. MD simulations aim to fill this gap. The ultimate

* Helium ions pick up electrons from the film as they approach it. When helium ions are mentioned in this thesis, they may sometimes be helium atoms instead.

purpose is to understand at an atomic level what goes on during film growth and ion irradiation. This is not without difficulties however. The MD simulations presented in this thesis never involve more than 12000 atoms and simulation times never exceed 12 ns (due to limited CPU power). This is far insufficient to produce a TDS spectrum, but the simulations do provide very detailed information about every atom in the simulation at practically any time during the simulation. Therefore the simulations are a useful tool to investigate the sometimes very complicated atomic mechanisms and short time events, such as argon trapping, helium implantation, sputtering etc. Some events that in real life would require more time can be simulated by applying some 'tricks', such as increasing the deposition rate to complete the deposition of a film within feasible simulation times, or increasing the film temperature to speed up diffusion. Although this increases the number of phenomena that can be studied, there are still some strong limitations. The tricks compromise the physical reliability if they are carried too far. Also, since atoms are treated as single, elementary particles, it is impossible to study properties that are governed by the behaviour of electrons, such as optical, magnetic, electrical and thermal transport properties. There is some justification for using Newtonian mechanics in the agreement between classical MD results and ab-initio calculations, although there is also some disagreement [1]. Because of their simplicity and computational efficiency, MD calculations have become widely accepted as a research tool. For example, Wang *et al* [2] have calculated fracture in amorphous silica using two- and three body potentials and Carlberg *et al* [3] have calculated simulations to study defect generation in epitaxial Mo/W superlattices using the Johnson-Oh Embedded Atom Method and Lennard-Jones pair potential. Still, despite their wide range of applications, MD simulations are limited to those 'mechanical' experiments in which the knowledge of individual electron states is unimportant, such as the study of atomic movement and ion-solid interactions. The interactions between molybdenum atoms used in this thesis do contain some information about the electronic structure of molybdenum in a simplified way. The interactions between atoms, the implementation of a MD simulation on a computer, and the possibilities and limitations are further discussed in chapter 2.

The main subjects of the simulations in this thesis are the influence of certain deposition parameters on film growth (deposition angle and energy, film temperature, argon energy, and ion to atom ratio), the effects of annealing, and the events taking place after argon and helium ion impacts. Because of limited CPU power it is not possible to simulate all possible combinations of parameters. Most combinations have been chosen in such a way to form pairs between which only one parameter is varied. This means that some conclusions may only be valid under certain circumstances. For instance, the influence of film temperature during deposition has only been investigated for (110) PVD* films. A partial list of simulations calculated for this thesis is included in chapter 3.

Chapter 4 contains the results of the simulations. Readers who are just interested in the results are advised not just to read chapter 4, because some results are influenced by the simulation conditions and not taking these into account will lead to erroneous conclusions. Reading at least also sections 2.1, 2.2, 2.3.1, 2.3.5, and the conclusions in chapter 5 is strongly recommended.

This thesis includes a CR-ROM. It contains the text and figures of this thesis in Word 6.0 and PDF formats, a number of Quicktime movies, a number of MacMolecule files, installers for the Adobe Acrobat Reader for MacOS, linux, various UNIXes and MS-Windows, the MacMolecule and PCMolecule program demos, the Xanim movie viewer for linux (it may also work on various UNIXes, but this was never verified), a tar archive containing the Camelion MD code used to calculate the results in this thesis with some examples, and a readme file describing the contents of the MacMolecule files and Quicktime movies.

The movies show the evolution of films during growth, the annealing of films and the effects of ion impacts. The MacMolecule files are 3D impressions of the molybdenum films, which can be manipulated (e.g. rotated, atom-coloured according to a number of criteria, etc.). The movies and MacMolecule files have been included because some results

* PVD in this thesis means atoms deposited by electron beam evaporation without argon ion assistance.

are better explained by moving images than by words or a small number of pictures. Most of the Quicktime movies are cinepack-compressed and they can be displayed on any Macintosh system that has the Quicktime extensions installed (available from www.apple.com/quicktime). Most of them can also be displayed on MS-Windows systems that have the Quicktime extensions installed (also available from www.apple.com/quicktime for Windows), and on linux and (possibly) various UNIXes, using Xanim. The MacMolecule files can be viewed by the MacMolecule demo on Macintosh systems and the PCMolecule demo on MS-Windows systems. The full versions of MacMolecule and PCMolecule are available from Molecular Ventures inc., URL www.molvent.com. The full MacOS version has the capacity to record Quicktime movies.

Enjoy.

2 Molecular dynamics

2.1 General principles

The principles of a classical molecular dynamics simulation are quite straightforward. It is simply a matter of solving Newtons equations of motion for a number of atoms. All that is needed for this is an initial list of the positions and velocities of the atoms in the system and a description of particle interactions (see section 2.2). These interactions determine the forces acting on the atoms and since the masses of the atoms are known, their accelerations can be calculated. Positions, velocities and accelerations are enough to determine the time evolution of the system.

Once the state of the system (determined by just a list of positions and velocities, called a configuration) is known at a particular time, all other information about the system at that time can be calculated. For instance, the temperature can be calculated simply by determining the average kinetic energy from the velocities.

The equations governing a molecular dynamics simulation are

$$\boldsymbol{F}_i = -\frac{\partial U}{\partial \boldsymbol{r}_i}, \tag{1}$$

$$\boldsymbol{a}_i = \frac{\boldsymbol{F}_i}{m_i}, \tag{2}$$

where $\boldsymbol{F}_i$ is the force acting on atom i, U is the total potential energy of the system, $\boldsymbol{r}_i$ is the position of atom i, $\boldsymbol{a}_i$ is the acceleration of atom i, and m_i is the mass of atom i. When a particular form has been chosen to describe the interactions (see section 2.2), eqns. (1) and (2) can be rewritten in a more explicit form.

2.2 Interaction potentials

The time evolution of a system starting from an initial configuration is determined by the interactions between the atoms. Therefore it is very important that the interactions are an accurate model of how real atoms interact.

In this thesis low energy Mo-Mo interactions are modelled by the Embedded Atom Method (EAM). This method was chosen because EAM provides a more accurate description than pair potentials for systems containing pronounced defects, such as vacancies, vacancy clusters, and free surfaces [1]. EAM is based on the idea that one part of the potential energy of an atom is determined by a contribution from a pair potential and that the other part is determined by the electron density in which the atom is embedded. The equation describing the EAM is

$$U = \sum_{i=1}^{N} F_i(\rho_i(\boldsymbol{r}_i)) + \frac{1}{2}\sum_{i=1}^{N}\sum_{j=1, j\neq i}^{N} \phi_{ij}(r_{ij}), \tag{3}$$

in which F_i is the embedding function, i.e. the function that describes how the electron density part of the potential energy of atom i at position $\boldsymbol{r}_i$ depends on the electron density ρ_i at that position, and ϕ_{ij} is the pair potential contribution of two atoms i and j separated by a distance r_{ij}.

The electron density is derived from atomic wave functions, with some strong simplifications. The angular dependence of the wave function is averaged out. Consequently the electron density that one atom experiences only depends on the distances

to other atoms. The total density at a certain point is calculated by simply adding densities contributed by different atoms,

$$\rho_i = \sum_{j=1; j \neq i}^{N} f_j(r_{ij}), \tag{4}$$

where f_j is the electron density contributed by atom j at the position of atom i.

Based on a comparison between different EAM models made by Morishita and De la Rubia [4] for bcc vanadium the Johnson-Oh EAM [5] potential was chosen. Johnson and Oh have proposed the following general expressions for the embedding function, the electron density distribution, and the pair potential for a number of bcc metals:

$$F(\rho) = -\left(E_C - E_{1V}^{UF}\right)\left[1 - \ln\left(\frac{\rho}{\rho_e}\right)^n\right]\left(\frac{\rho}{\rho_e}\right)^n, \tag{5}$$

$$f(r) = f_e\left(\frac{r_{1e}}{r}\right)^{\beta}, \tag{6}$$

$$\phi(r) = K_3\left(\frac{r}{r_{1e}} - 1\right)^3 + K_2\left(\frac{r}{r_{1e}} - 1\right)^2 + K_1\left(\frac{r}{r_{1e}} - 1\right)^1 + K_0, \tag{7}$$

in which

$$n = \sqrt{\frac{9\Omega B - 15\Omega G}{\beta^2\left(E_C - E_{1V}^{UF}\right)}}, \tag{8}$$

$$K_3 = -\frac{15\Omega G}{3A + 2}\left(\frac{3}{4}A - \frac{1}{2}S\right), \tag{9}$$

$$K_2 = -\frac{15\Omega G}{3A + 2}\left(\frac{15}{16}A - \frac{3}{4}S - \frac{9}{8}AS + \frac{7}{8}\right), \tag{10}$$

$$K_1 = -15\Omega G\left(\frac{7}{8} - \frac{3}{4}S\right), \tag{11}$$

$$K_0 = -\frac{15\Omega G}{3A + 2}\left(\frac{201}{112}A - \frac{27}{28}S - \frac{87}{56}AS + \frac{187}{168}\right) - \frac{1}{7}E_{1V}^{UF}, \tag{12}$$

in which

$$S = \frac{r_{2e}}{r_{1e}}, \tag{13}$$

$$A = \frac{2C_{44}}{C_{11} - C_{12}}, \tag{14}$$

$$G = 3C_{44} + C_{11} - C_{12}. \tag{15}$$

In these equations E_C is the cohesive energy, E_{1V}^{UF} is the unrelaxed monovacancy formation energy, ρ_e is the (dimensionless) equilibrium electron density, f_e is a dimensionless factor that cancels out for single-element potentials, r_{1e} and r_{2e} are the first and second equilibrium neighbour distances, β is a constant (of little influence, a value of 6 was chosen by Johnson and Oh), Ω is the atomic volume, B is the bulk modulus, G is the Voigt average shear modulus, and C_{11}, C_{12}, and C_{44} are the cubic elastic constants.

The cohesive energy, equilibrium lattice constant a, the three elastic constants, and the unrelaxed monovacancy formation energy are the input parameters for the potential. The values used for constructing a bcc Mo-Mo EAM potential are given in table I [5]. Note that for the lattice constant a more accurate value is used that differs slightly from the value of 3.150 Å used by Johnson and Oh.

Table I. Values used for constructing the EAM potential for bcc molybdenum. The values are the lattice parameter a, atomic volume Ω, the bulk modulus B, the Voigt average shearmodulus G, the anisotropy ratio A, the cohesive energy E_C, and the unrelaxed monovacancy formation energy E_{1V}^{UF}.

quantity	
a (Å)	3.1472
B (eV)	25.68
G (eV)	12.28
A	0.78
E_C (eV)	6.81
E_{1V}^{UF} (eV)	3.1

The embedding function of eqn. (5) is very steep near =0, the derivative tends to -∞. As a result of discretization errors (see also section 2.3.4) this singularity can produce unreliable results. To alleviate this problem, the embedding function has been multiplied by the function

$$h(\rho) = 1 - e^{-\frac{1}{2}\left(\frac{\rho}{\rho_s}\right)^2} , \qquad (16)$$

in which $_s$ was given the value 0.5. This fixes the problem with the singularity. There is no theoretical basis for doing this, but only the low-density part of the embedding function is significantly affected. The embedding energy for low densities is small, consequently reducing it further or increasing it by a small fraction has no significant impact. The Mo embedding function is shown in fig. 1.

The electron density function has also been altered slightly from eqn. (6) to limit the radial range and thereby the number of interactions. This is done by substituting for large distances $r_s < r < r_c$ the density function $f(r)$ by the function $f_c(r)$ given by

$$f_c(r) = \frac{-2f(r_s) + (r_s - r_c)f'(r_s)}{(r_s - r_c)^3}(r - r_c)^3 + \frac{3f(r_s) - (r_s - r_c)f'(r_s)}{(r_s - r_c)^2}(r - r_c)^2 . \qquad (17)$$

This function has the properties $f_c(r_s) = f(r_s)$, $f_c'(r_s) = f'(r_s)$, $f_c(r_c) = f_c'(r_c) = 0$. Therefore the corrected function smoothly connects to the original function at r_s and then gradually

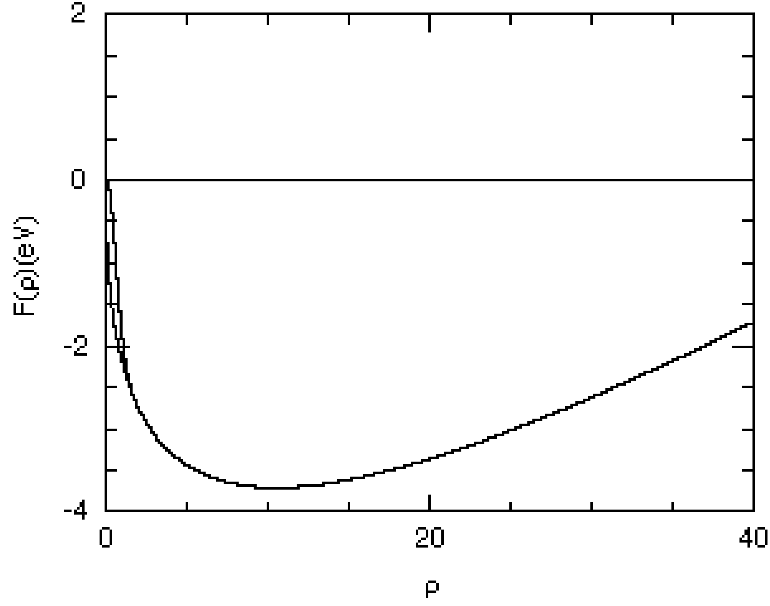

Figure 1. Embedding function F versus electron density ρ for Mo.
The solid curve represents the embedding function used in simulations.
The dashed curve is the unmodified embedding function (eqn. (5)).

goes to zero at r_c. For r_s and r_c the values $r_{2e} + 0.1*(r_{3e} - r_{2e})$ and $r_{2e} + 0.5*(r_{3e} - r_{2e})$ were chosen, in which r_{3e} is the third equilibrium neighbour distance. This limits the number of interactions to an average of 14, the sum of the number of nearest and next-nearest neighbours. The pairpotential has been treated in a similar manner. A second modification of the electron density function, at short distances, will be discussed later.

Since the Johnson-Oh EAM is derived for low energy situations, different potentials are used for short distances. For distances smaller than 2.70 Å the Johnson-Oh pair potential is stiffened. Instead of $\phi(r)$ one should use $\phi_S(r)$, given by

$$\phi_S(r) = \phi(r) + 4.5\left(1 + \frac{4}{A - 0.1}\right)\left(\phi(r) - \phi(r_{1e})\right)\left(\frac{r}{r_{1e}} - 1\right)^2 . \tag{18}$$

For distances smaller than 1.59 Å the Screened Coulomb pair potential with Molière weight factors and Firsov screening length [6] is used. This purely repulsive potential has the form

$$\phi(r) = \frac{Z_1 Z_2 e^2}{4\pi\varepsilon_0 r}\gamma\left(\frac{r}{a}\right) , \tag{19}$$

in which

$$\gamma\left(\frac{r}{a}\right) = \sum_1^3 c_i e^{-d_i \frac{r}{a}} , \quad \sum_1^3 c_i = \gamma(0) = 1 , \tag{20}$$

and

$$a = \left(\frac{9\pi^2}{128}\right)^{\frac{1}{3}} a_B \left(Z_1^{\frac{1}{2}} + Z_2^{\frac{1}{2}}\right)^{-\frac{2}{3}}, \tag{21}$$

in which Z_1 and Z_2 are the atom numbers of the interacting particles at distance r, e is the elementary charge, $_0$ is the vacuum permittivity, γ is the screening function, a is the screening length, c_i and d_i are constants, and a_B is the Bohr radius. The Molière values for c_i and d_i are given in table II.

Table II: Molière constants in the screening function.

i	c_i	d_i
1	0.35	0.3
2	0.55	1.2
3	0.10	6.0

Since the EAM potential is based on a combination of a pair potential and an electron density and the Screened Coulomb potential is a pure pair potential, a method has to be devised to smoothly go from one potential to the other. In other words, the electron density function should fall off to zero when the distance from the nucleus decreases towards the range where the Screened Coulomb pair potential takes effect. This is done by multiplying $f(r)$ with a Fermi-Dirac-like function,

$$g(r) = \frac{1}{e^{\frac{r_z - r}{r_z}} + 1}, \tag{22}$$

in which r_z is a constant that determines where the function is equal to 1/2 and r_z is a constant that determines how steeply the function rises from 0 to 1. For r_z and r_z the values of 1.8 Å and 0.025 Å were chosen. In this way the electron density and hence the embedding energy are practically zero near the atom core. The stiffened Johnson-Oh and Screened Coulomb pair potentials have been smoothly connected in the r-range where their values are almost the same (1.59 to 2.08 Å). At the transition radius from EAM interaction to pure pair interaction the electron density interaction is not as repulsive as the original EAM potential as a result of this modification of the electron density. This causes a small shoulder in the potential. This error has to be accepted in going from the EAM potential to the pair potential. The Mo electron density distribution and Mo-Mo pair potential for low electron densities and energies have been plotted in figs. 2 and 3. For an isolated system of two molybdenum atoms the potential well shape for an isolated pair of atoms is depicted in figure 4. The potential well only has this shape in the absence of other atoms. In the presence of, for example, a third atom at a constant distance from the other two, the well will not only be shifted up or down, but it will also change shape due to the extra electron density contribution of the third atom.

All results in this work have been calculated using the modified Johnson-Oh EAM potential in combination with the Firsov-Molière Screened Coulomb potential, unless mentioned otherwise. A few simulations have been calculated using a different, Finnis-Sinclair EAM potential without modifications. This potential is described in [7].

For noble gas interactions the Firsov-Molière Screened Coulomb pair potential has been used with the values in table II. No attractive potential was added to this purely repulsive potential. This is justified because the noble gas atoms are practically always in high-energy situations where neglecting a few meV of binding energy has no influence.

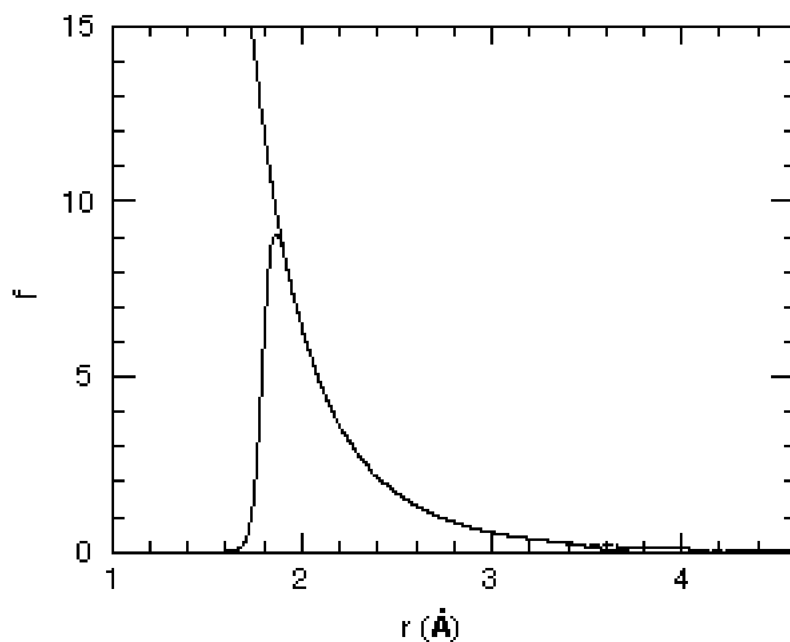

Figure 2. Electron density f versus distance r for Mo. The solid curve represents the electron density used in simulations. The dashed curve is the unmodified density (eqn. (6)).

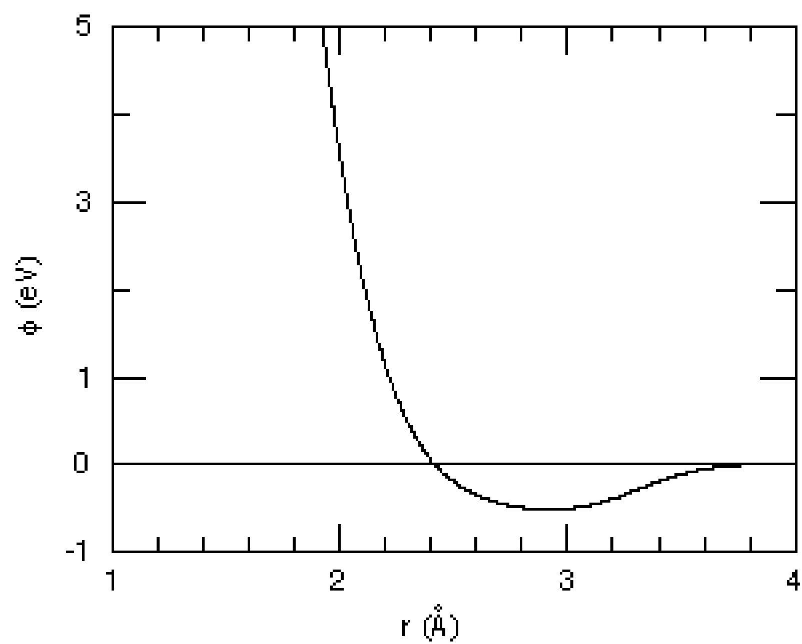

Figure 3. Mo-Mo pairpotential ϕ versus distance r for low energies.

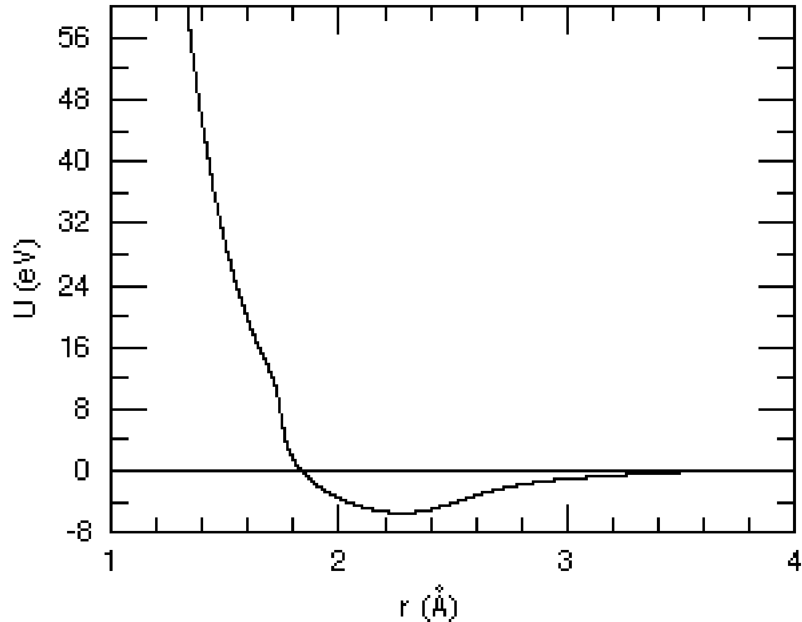

Figure 4. Potential energy U of an isolated pair of Mo atoms at a distance r. Note the shoulder in the transition region around $r = 1.8$ Å.

2.3 Implementation on a computer

2.3.1 The system in a box

CPU power today is still insufficient to simulate the length and time scales of real Ion Beam Assisted Deposition (IBAD) experiments. Computers used to calculate the results in this thesis need a few months to simulate 10000 atoms for 10^{-8} s. Ten thousand atoms form a cube only about 50 Å big. In order to give the impression of a large specimen using only a small number of atoms, a simulation box with periodic boundary conditions is used. This means that the system is considered to repeat itself after a certain length (so atoms at position $\mathbf{R}$ are also present at positions $\mathbf{R} + \mathbf{L}_x$, $\mathbf{R} - \mathbf{L}_y$, $\mathbf{R} + 2\mathbf{L}_x - 3\mathbf{L}_y$ etc. where $\mathbf{L}_x$ and $\mathbf{L}_y$ are the length vectors of the box edges). This effectively removes unphysical boundary effects, see fig. 5. On the other hand, the periodic lengths impose restrictions on the phenomena that can be studied. For instance, nucleation from a melt will never occur if the volume of the system is smaller than the critical nucleus size. Apart from the limited size there is also the short simulation time. These and other limitations are discussed in section 2.5.3.

In the direction perpendicular to the film periodic boundary conditions are useless because depositing atoms requires a free surface, so it appears as if only thin films not attached to bulk material can be studied. This would in turn cause two problems: heat from incoming particles cannot diffuse out of the system into a substrate and the momentum from incoming atoms would eventually cause the film to drift away. For this reason atoms in the two lowest atomic planes are given a special treatment in the simulations to overcome these problems [8]. These 'bottom atoms' experience a force not only from the interactions with other atoms but also from an artificial harmonic force which ties these atoms to their specified equilibrium positions. This harmonic force prevents the film from drifting away. The bottom atoms can also be used to remove excess energy. This is done by scaling their

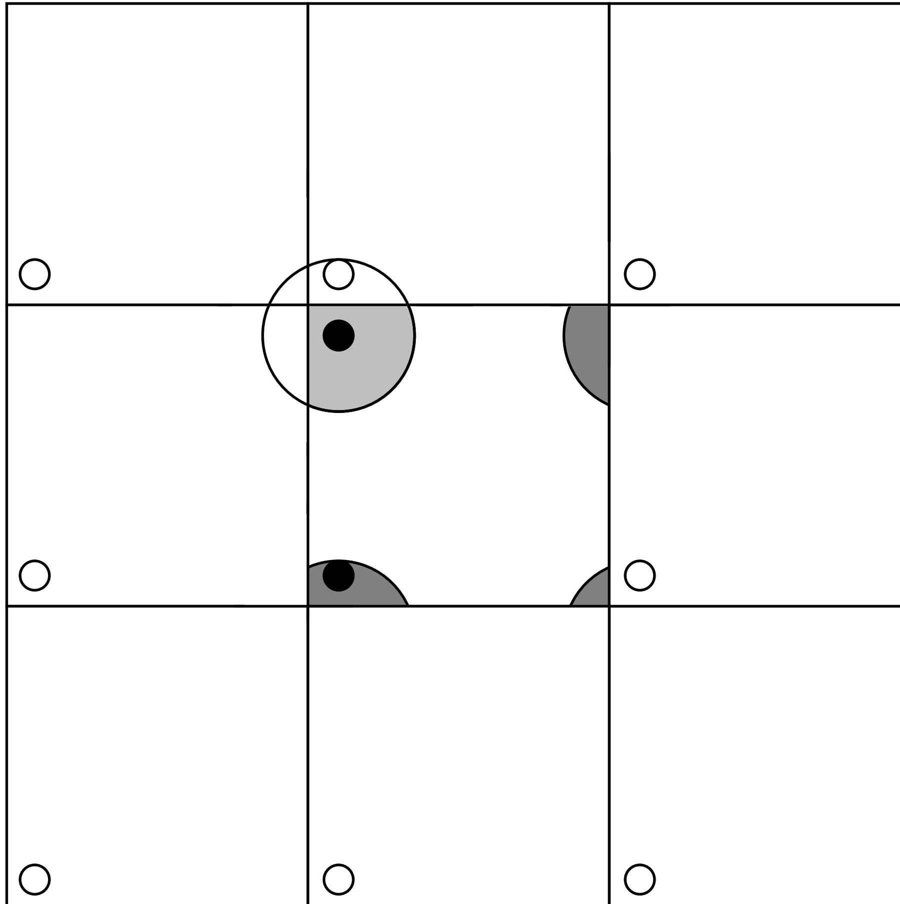

Figure 5. Schematic representation of periodic boundary conditions. The upper black atom, shown with its interaction range, interacts with all atoms in the hatched area, but also with the atoms in the shaded areas through their periodic images in the adjoining boxes. The computer calculates all interactions only once, of course.

velocities in such a way that a preset temperature T_{bot} can be maintained and by temporarily disabling the harmonic force on atoms whose velocity perpendicular to the film is directed towards the film and whose kinetic energy exceeds $1/2*kT_{bot}$. The first selection criterion ensures that the harmonic force is disabled only if atoms are moving towards the film, ensuring that the bottom atoms can never be detached from the film. The second selects those atoms that are 'too hot'. In effect, these atoms are given a lower potential energy without being accelerated by the harmonic force, thus removing energy from the system.

The non-periodicity perpendicular to the film allows for the deposition of thicker films using the 'cut and shift down' method. This method works as follows: deposition in a simulation box is continued until the box is nearly full. Then the film is cooled to near 0 K and the bottom part of the film is cut away. The rest of the film is shifted down. Atoms in what are now the lowest two planes become bottom atoms. Because the film has been cooled to near 0 K their equilibrium positions are known. The system is reheated to its original temperature and deposition is continued. This method can be applied when diffusion in the lower part of the film is negligible (which it usually is, see section 4.5.2).

Atoms can be introduced at the top of the box, with specified energy and angles of incidence. The positions for introduction are selected by a random number generator. Particles that move out of the box through the top (or sometimes through the bottom) are assumed no longer to be of interest to the simulation and are removed from the system. A

record is kept containing information about the angles, energies, positions, and time at which particles are introduced and removed.

2.3.2 Numerical algorithm

Eqn. (1) can usually not be solved analytically for a system of thousands of atoms. Therefore the widely used Velocity-Verlet algorithm [9] is used to produce a numerical approximation. From atomic positions $\boldsymbol{r}$, velocities $\boldsymbol{v}$, and accelerations $\boldsymbol{a}$ at time t the algorithm first calculates the new positions at time $t + \quad t$,

$$\boldsymbol{r}(t + \quad t) = \boldsymbol{r}(t) + \boldsymbol{v}(t) \quad t + \frac{1}{2}\boldsymbol{a}(t)(\quad t)^2, \tag{23}$$

where $\boldsymbol{a}$ is determined from the positions of the atoms using eqn. (2), and from these new positions the new accelerations $\boldsymbol{a}(t + \quad t)$ are calculated. The velocities at $t + \quad t$ are calculated in two steps:

$$\boldsymbol{v}(t + \frac{1}{2} \quad t) = \boldsymbol{v}(t) + \frac{1}{2} \quad t\boldsymbol{a}(t), \tag{24}$$

$$\boldsymbol{v}(t + \quad t) = \boldsymbol{v}(t + \frac{1}{2} \quad t) + \frac{1}{2} \quad t\boldsymbol{a}(t + \quad t). \tag{25}$$

When positions, velocities, and accelerations at $t + \quad t$ are known, the process can be repeated to calculate the next configuration.

The timestep $\quad t$ is not a constant in a simulation run. Timestep control is discussed in the next section.

2.3.3 Timestep control

The timestep $\quad t$ should be chosen in such a way that no atom moves more than a small distance $\quad r$ over which the forces on the atoms do not change significantly. In this way, the numerical result after $\quad t$ will be a close approximation of the analytical result. An accurate criterion for the magnitude of $\quad r$ would involve the computation of countless forces with atoms at various trial positions. As this would lead to excessive computer time, we have followed the usual approach of using a fixed distance limit $\quad r \quad R$. R is chosen in such a way that even in the situation in which $\mathrm{d}\boldsymbol{F}/\mathrm{d}\boldsymbol{r}$ has its highest value, the forces on the atoms do not change significantly over a distance R. In the simulations used to calculate the results in this thesis the value $R = 0.020$ Å was chosen.

During IBAD simulations, velocities of atoms vary over a very broad range. Therefore a constant timestep is impractical, because the timestep would always have to be so small that the fastest atom of the *entire simulation* does not move more than $\quad r$. Because of this, a variable timestep is chosen, allowing the fastest particle of *one configuration* to move a distance R. That way, a much larger timestep can be used for most configurations, because only few configurations contain very fast atoms. Another way to improve efficiency is to exclude atoms from limiting the timestep as long as they are in free flight.

The algorithm to determine the timestep in this way is somewhat complicated. The general idea for timestep control with variable timestep and free flight algorithm is as follows:

- for the first atom in a loop over all atoms experiencing a force ($\boldsymbol{a} \neq 0$), the distance Δr that it will move away from its starting point during an initial trial timestep[*] Δt is calculated using eqn. (26),[**]

$$(\Delta r)^2 = v^2(\Delta t)^2 + (\boldsymbol{a} \bullet \boldsymbol{v})(\Delta t)^3 + \frac{1}{4}a^2(\Delta t)^4. \tag{26}$$

  The acceleration is included in eqn. (26) because for atoms with a small velocity, for instance close to ultimate collision impact, it can contribute significantly to Δr and neglecting it could result in a very inaccurate approximation for systems with small numbers of atoms (neglecting (**a•v**)(Δt)^3 + 1/4*a^2*(Δt)^4 will result in a timestep that is too long. In systems of thousands of atoms this is not important because there will always be other atoms that limit the time step. However, theoretically, in systems with few atoms, such as two-particle systems used in accuracy tests, situations can arise in which any time step could be selected).
  Depending on whether this distance is smaller or larger than R, Δt is increased or decreased and Δr is calculated again for the atom under consideration. This process is repeated until Δr corresponds to R.[***]
- for the other atoms experiencing a force, the travel distance Δr in time Δt of the previous atom is calculated and if it exceeds R, Δt is further reduced. This establishes a first estimate of Δt.
- free atoms ($\boldsymbol{a}$ =0) are allowed to travel an unlimited distance, but only for as long as they do not come near other atoms during the trial timestep. If they do, the trial time is further reduced to allow them to come just inside the influence of another atom.
- atoms for which the cosine of the angle between $\boldsymbol{a}$ and $\boldsymbol{v}$ is smaller than $-\sqrt{8/9}$ are treated in a special way. The criterion cos($\boldsymbol{v}, \boldsymbol{a}$) < $-\sqrt{8/9}$ selects those atoms whose velocity and acceleration point almost exactly in opposite directions. These atoms are about to 'make a turn'. This requires a special approach because the distance they travel away from their starting points is not a monotonously increasing function of Δt.. This can be seen as follows. From eqn. (26) we get

$$\frac{\mathrm{d}\left((\Delta r)^2\right)}{\mathrm{d}(\Delta t)} = 2v^2 \Delta t + 3(\boldsymbol{a} \bullet \boldsymbol{v})(\Delta t)^2 + a^2(\Delta t)^3. \tag{27}$$

  $(\Delta r)^2$ is not a monotonous function of Δt if there are real, non-zero roots for the equation

$$\frac{\mathrm{d}\left((\Delta r)^2\right)}{\mathrm{d}(\Delta t)} = 0 \Rightarrow a^2(\Delta t)^2 + 3(\boldsymbol{a} \bullet \boldsymbol{v})\Delta t + 2v^2 = 0. \tag{28}$$

  In general, the roots Δt_1 and Δt_2 of eqn. (28) are

$$\Delta t_1,\ \Delta t_2 = -\frac{3(\boldsymbol{a} \bullet \boldsymbol{v})}{2\boldsymbol{a}^2} \pm \sqrt{\frac{9(\boldsymbol{a} \bullet \boldsymbol{v})^2}{4(a)^4} - 2\frac{\boldsymbol{v}^2}{\boldsymbol{a}^2}}. \tag{29}$$

---

[*] In the first configuration an arbitrary value is used. In the configurations after that, the ending value of the previous configuration is used as initial trial time.

[**] The square of Δr is used because calculating square roots is then avoided. Calculating square roots is a time consuming operation for a CPU.

[***] It is possible to determine the desired value of Δt exactly by solving eqn. (24) for $\Delta r = R$, but this involves calculating a number of square roots.

So $(\Delta r)^2$ is not a monotonous function if

$$\frac{9(\boldsymbol{a}\bullet\boldsymbol{v})^2}{4(a)^4}-2\frac{v^2}{a^2}>0\,, \tag{30}$$

which finally leads to $\cos(\boldsymbol{v},\boldsymbol{a}) < -\sqrt{8/9}$ and $\cos(\boldsymbol{v},\boldsymbol{a}) > \sqrt{8/9}$. The second solution corresponds to a negative timestep and does not need to be considered.

What does all this mean? Fig. 6 shows two examples of $(\Delta r)^2$ as a function of t.

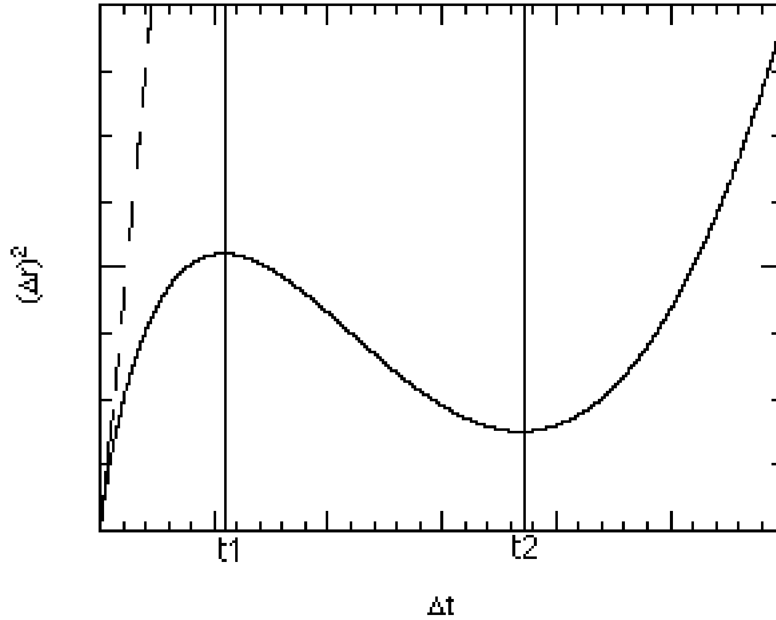

Figure 6. $(\Delta r)^2$ as a function of t for a case (dashed curve) in which $\cos(\boldsymbol{v},\boldsymbol{a}) > -\sqrt{8/9}$ and a case (solid curve) in which $\cos(\boldsymbol{v},\boldsymbol{a}) < -\sqrt{8/9}$.

The dashed curve is an example in which $\cos(\boldsymbol{v},\boldsymbol{a}) > -\sqrt{8/9}$. In this case, $(\Delta r)^2$ increases monotonously with t. If the procedure described above is followed, $(\Delta r)^2$ will always correspond to the desired R^2 after a number of iterations, no matter what the initial value of t is. The full curve is an example where $\cos(\boldsymbol{v},\boldsymbol{a}) < -\sqrt{8/9}$. The curve has a local maximum at t_1 and a local minimum at t_2. If this is the case, three situations can be distinguished, depending on the value of R^2. In the first situation R^2 is smaller than the minimum of $(\Delta r)^2$ at t_2, in the second situation R^2 lies between the minimum at t_2 and the maximum at t_1, and in the third situation R^2 is larger than the maximum at t_1. These three situations and the situation where $\cos(\boldsymbol{v},\boldsymbol{a}) > -\sqrt{8/9}$, mentioned above, are illustrated in fig. 7. Trajectory 1 in fig. 7 corresponds to the situation in which R^2 is smaller than the minimum at t_2. In this case the correct value for t will always be found. For trajectory 2 this is not the case. If the initial trial time is large, the computer could select point B or C, points the atom passes on its way back after it has made the turn. It should select point A. This is done by limiting the timestep to t_1 and reducing it further as needed. Atoms with type 3 trajectories should also be treated differently. These atoms never move more than a radial distance R away from their starting point, but they can travel a total length of up to $3R$, see fig. 8.

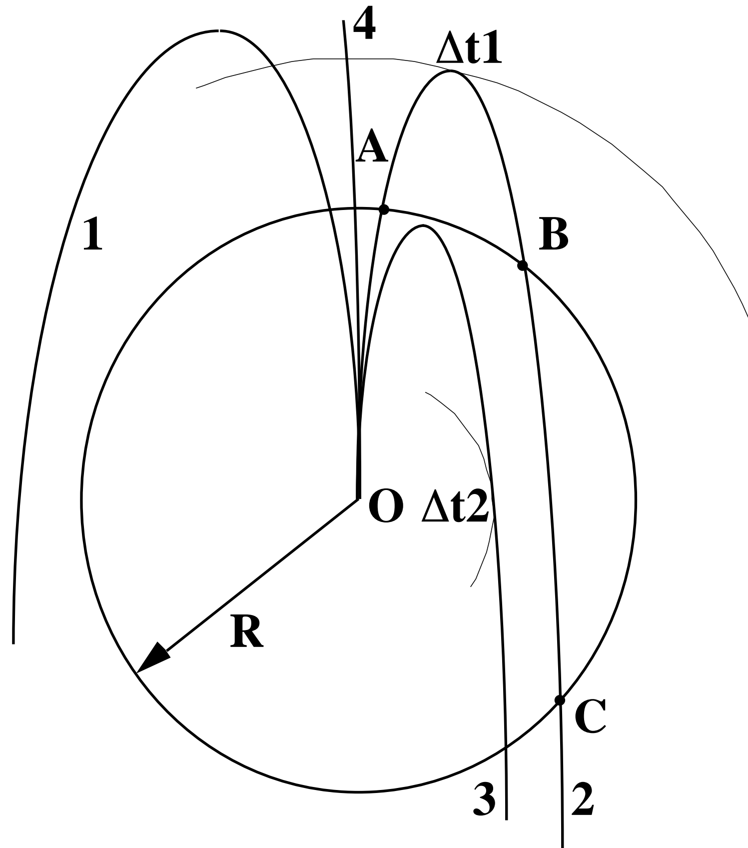

Figure 7. Four possible trajectories of an atom starting at point O. Trajectory 1 belongs to an atom that is about to 'make a turn' in the sense considered here ($\cos(\boldsymbol{v},\boldsymbol{a}) < -\sqrt{8/9}$), but not in this timestep yet. Trajectory 2 belongs to an atom that is about to make a turn after the time interval denoted as t_1, , but the turning point is outside the allowed travel distance R. Trajectory 3 belongs to an atom that makes a turn before travelling a distance R away from the starting point. Trajectory 4 belongs to an atom for which $\cos(\boldsymbol{v},\boldsymbol{a}) > -\sqrt{8/9}$). In this case, there is always just one intersection between the trajectory and the circle with radius R, no matter how large R is chosen.
t_1 and t_2 are the roots of eqn. 29.

A distance of $3R$ is too long and therefore the timestep is set to t_2.
Finally, if the timestep selected for an atom exceeds the trial time of the previous atom, the previous trial time is not reduced.

The actual algorithm involves many more steps and choices. The Fortran code used to determine the timestep is included in appendix A.

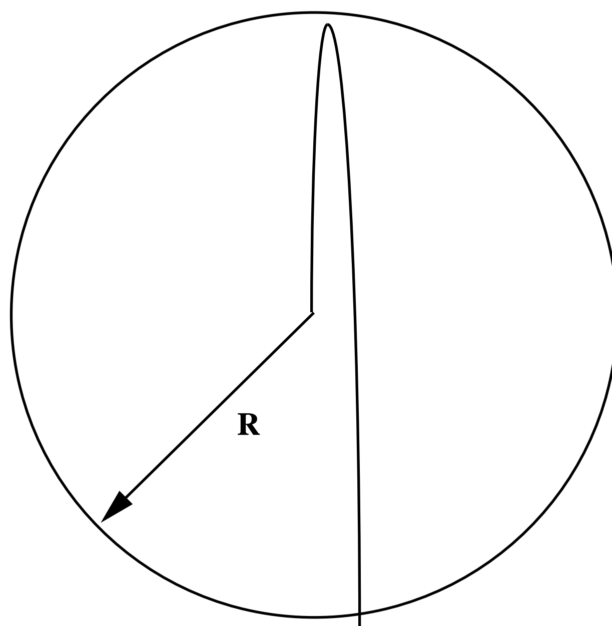

Figure 8. Orbit of an atom with type 3 orbit. The atom never moves further than a distance *R* away from its starting point, but it can travel a total distance of up to 3*R*.

2.3.4 Accuracy, numerical stability, and reproducibility

Since the trajectories are calculated by a numerical approximation and are stored in a limited number of digits, a small error is made in each timestep. The relative error is small, $0.5*10^{-8}$ for single precision numbers and $0.5*10^{-16}$ for double precision numbers if rounding is carried out correctly and according to the same algorithm on all machines (which seems questionable sometimes). However, these small errors accumulate during successive steps and after a number of steps, the numerical trajectories start to diverge significantly from the true trajectories. Therefore there is no way of saying that an atom is within a certain distance of its analytical position, because sometimes it will be in a different lattice position. Things are made worse by storing a configuration on disk, halting the simulation, and then restarting it. This introduces an inaccuracy because either not all information is stored on disk (even if the maximum number of digits is stored), or it is not properly reloaded into memory when the simulation is resumed. When a simulation of 10000000 steps is calculated in one run or when it is calculated in two runs of 5000000 steps, the results are different. Also, in the course of the work described in this paper, a number of bugs have been fixed, again making reproducibility impossible. The final blow to reproducibility is given by small changes in the code to fix bugs and the large number of different compilers, operating systems, and CPUs that have been used[*]. Runs on different systems produce different results. Starting from the same initial configuration, the temperature, for example, will first differ (a relative error of 10^{-8} for single precision data) on different machines after about 400 configurations.

All things mentioned in the previous paragraph may seem disastrous to doing molecular dynamics. Fortunately it is not as bad as it may seem. Atoms at different positions do not necessarily mean different results in the sense that the physics on one computer is different from that on another. Macroscopic properties such as the roughness of the surface or average properties such as the percentage of vacancies are very similar on

[*] The simulations have been calculated with f77 for Irix 5.3/6.2 on Mipps R4400, f2c+gcc for Red Hat linux on pentium 100, 120, 200 and 233MMX, g77 for Red Hat linux on pentium 100, 120, 200 and 233MMX, f2c+gcc for Mklinux on PowerPC 601 and 604e, f77 for OSF unix on DEC Alpha and f90 for Unicos 9.2 on a Cray J90 supercomputer.

different systems, even if the films look slightly different. Different results on different machines are merely different ways of telling the *same* story.

2.3.5 Box size, heat conduction, and simulation timescale

Apart from numerical considerations there are a number of other things to keep in mind. The box size limits the size of the phenomena that will occur and the energy of incoming particles. The size limit is important because a small box size may suppress things that would take place in an experiment, or may cause unrealistic things to happen. For instance, a box of 3 by 3 atoms will never develop a columnar structure because the boundary between 2 columns alone is a few atoms wide. Simulations in a much larger box do allow a columnar structure to develop. This also shows the limitations of the cut and shift down method. In a real thick film the size of features parallel to the film may grow with the film thickness. This growth would be unrealistically suppressed is a thick film was grown from a very small box by repeatedly using the cut and shift down method. Even if certain features do fit into the box, their existence may still be suppressed. For instance, a standing wave with a wavelength of 70 Å can not subsist in a 90 Å box.

The box size limits the energy of incoming particles because the heat from the impact may interact with itself through the periodic boundary if the energy is too high. Perpendicular to the film kinetic energy may reflect from the bottom atoms in an unrealistic way. Small particles may also pass through the film if the thickness is too small. Most boxes used in this work were about 45 x 45 x 45 Å. The maximum energies used in the simulations are 250 eV for Ar ions and 100 eV for helium ions. At these energies there is already a small ‘spill-over’ of energy into the next box images sometimes, and a few helium ions have been observed to pass through the film, indicating that higher energies should certainly not be used.

Things are further complicated by the lack of electronic heat conductance. This causes heat to diffuse away more slowly. After an ion impact, for instance, this may cause local melting to occur more frequent than is realistic.

The last thing that may cause physically unrealistic results is the short timescale of the simulation. In order to complete the deposition of a film in 10^{-8} s the deposition rate has been dramatically increased by a factor of over 10^{9} (the deposition speed is 0.5 m/s instead of the experimental value of 1 Å/s). This disables almost all diffusion processes during deposition and all effects concerning the evolution of for instance surface roughness are almost purely deposition effects. In order to study the influence of diffusion a number of annealing and deposition runs have been carried out at elevated temperatures. These runs show that the influence of diffusion is not very significant for the evolution of the topology of the film, but that it is important in other things, see section 4.3.4.

It is usually possible to estimate the influence of the above mentioned points, but it will be clear that care has to be taken in choosing the conditions for a simulation.

3 Scope of the simulations

The computer simulations in this thesis were done to complement the experimental IBAD research carried out in our group, although a number of simulations were calculated because they were interesting by themselves. For the last two years the experimental research has focused on depositing thin molybdenum films on molybdenum substrates, often assisted by argon ions [10]. The films are investigated by Thermal Desorption Spectrometry (TDS).

The simulations can be divided into four categories:

* Deposition of complete films. The purpose of these simulations was to investigate the influence of certain parameters of the deposition conditions:
  (A) The surface orientation has been investigated because a large difference in surface roughness between the (100) and (110) orientations was discovered [11]. A few simulations were also carried out on (111) surfaces.
  (B) The deposition angle in most simulations was 15° off-normal with a 13° angle from the in-plane (100) direction. The 15° angle was chosen because this is the experimental deposition angle. The 13° angle was chosen rather arbitrarily because experimentally this angle is not known (for single-crystalline samples) or varies from grain to grain (for polycrystalline samples). The angle was chosen in such a way that it did not lie along any low-index crystallographic direction. Some simulations were carried out with a 30° off-normal angle parallel to the in-plane (100) direction, and some a deposition angle perpendicular to the surface. As in the experiment argon ions always impinged perpendicular to the surface.
  (C) The Ion to Atom Ratio (IAR) was usually 0 (PVD) or 0.1, as in the experiments. One simulation with an IAR of 0.2 was done to investigate the influence of a higher IAR.
  (D) The energy of argon ions was 25, 100 or 250 eV as in the experiment. In the experiments, low-energy argon beams are often contaminated with a small fraction (0.1) of 250 eV argon ions. This small fraction of 250 eV ions has been included in most IBAD simulations.
  (E) The film thickness was usually about 40 Å, sometimes up to 70 Å, using the cut and shift down method, see section 2.3.1. Experimentally films up to a few hundred Å are deposited but there was insufficient CPU power and memory to simulate such thick films.
  (F) The deposition rate was usually $5*10^{9}$ Å/s, compared to 1 Å/s in experiments. A few simulations with a deposition speed of 10^{10} Å/s were calculated for comparison.
  (G) The substrate temperature was usually room temperature or slightly higher, as in the experiment. One simulation was carried out at 2000K to investigate the influence of diffusion.
* Decoration of defects with helium ions. As in the experiment films have been bombarded with 100 eV helium ions under a 20° off-normal angle. The helium fluence was usually $5*10^{14}$ helium ions/cm^2; one simulation was carried out with a $2*10^{15}$ ions/cm^2 fluence. The experimental fluence varies, but often it is $2*10^{14}$ ions/cm^2.
* Annealing completed films. A number of films have been annealed at 2000 or 1500 K. Because of the short simulation times it is impossible to obtain a helium or argon desorption spectrum by heating a film (the experimental heating rate is 40 K/s, whereas the heating rate in a simulation would be in the order of 10^{15} K/s). Therefore films were annealed at constant temperature, 1500 or 2000 K, in order to study processes taking place at elevated temperatures. These rather high temperatures (2000 K is the maximum temperature during a desorption measurement) are chosen to speed up thermally activated processes. A number of films containing vacancies, vacancy clusters (up to a few dozen vacancies), helium and/or argon ions, self-interstitials, and a dislocation loop have been annealed. Four perfect boxes (periodic in all directions) into which monovacancies were introduced at periodic positions have been annealed at 500, 1000, 1500, and 2000 K to investigate monovacancy mobility. Annealing times were up to 10 nanoseconds.
* Miscellaneous short simulations. Certain simulations were done to visualise certain events and determine activation energies, implantation profiles, and surface relaxation.

(A) When comparing two configurations of a deposition run, one can sometimes conclude that something interesting has happened during the time interval between the two configurations, for instance the creation of a vacancy cluster by an argon ion. In many of these cases the simulation has been restarted at the first configuration and saved to disk at very short time intervals in order to create a movie from the saved configurations. In this way a number of movies has been created that display events after argon and helium ion impacts. It is also possible to let the computer generate extra information about atoms that are of special interest.
(B) A simple way to determine activation energies is to cool a configuration to 0 K and give one atom enough energy to just enable it to move to the next lattice position. The minimum kinetic energy of all trial directions is the activation energy for migration. The application of this so-called cold method is limited. It can not be applied to bulk diffusion. This is because the method is not fully realistic: in reality the atom that is to move to the next position will probably do so when 'blocking' atoms have just moved out of the way a little. Atoms at near 0 K don't move out of the way. Therefore the activation energy will be too high (see also section 4.3.5). For surface diffusion this error is smaller than for bulk diffusion, because the moving atoms can move over the blocking atoms with only little extra energy, instead of having to push away the atoms in its path. Another objection of the application of the cold method is the neglection of the strong coupling of motion of neighbouring atoms.

Using the method above a number of migration energies have been determined. To check the validity of the method one migration energy has also been determined by simulating real diffusion of one atom over a flat surface.
(C) Ion implantation profiles can be determined by calculating a short simulation of an impinging ion and stopping the simulation as soon as the ion has reached a fixed position in a defect or in an interstitial position. This position and other information about the ion is stored. After this the same simulation is restarted, but with the ion starting at a different random position. From the positions where the ions are at their lowest points in the film, the implantation profile can be determined[*] . This has been done for 100 eV helium ions on a (100) surface and for a small number of 250 eV argon ions on a (110) surface.
(D) Surface relaxation has been studied by cooling a system with a free surface to near 0 K and measuring the distance between atomic planes.

[*] Note that implantation profiles are often determined from the positions where the kinetic energy of ions has dropped below a certain value, instead of the lowest position criterion used here.

4 Results

4.1 Verification and accuracy tests

A number of tests have been performed to verify the reproduction of the input parameters for the Mo-Mo potential, to check the stability of the bcc structure against the fcc structure, and to check the accuracy of the model and the program. The Voigt average shear modulus and anisotropy ratio have not been checked, because this was not practical with the Camelion MD code.

The results of simulations to test the reproduction of input parameters are given in table III.

Table III. Reproduction of input parameters. The original input parameters, lattice parameter *a*, atomic volume Ω, bulk modulus *B*, Voigt average shear modulus *G*, anisotropy ratio *A*, cohesive energy E_C, and unrelaxed monovacancy formation energy E_{1V}^{UF} at 0 K and the values (if determined) returned by simulations.

quantity	input value	returned value
a (Å)	3.1472	3.1472
B (eV)	25.68	25.88
G (eV)	12.28	-
A	0.78	-
E_C (eV)	6.81	6.81
E_{1V}^{UF} (eV)	3.10	3.19

From table III it can be concluded that the input parameters reproduce well, except for the unrelaxed vacancy formation energy. There is no explanation why this parameter has such a high relative inaccuracy compared to the others.

The difference in cohesion energy between fcc and bcc molybdenum has been determined to check bcc stability. Fcc molybdenum has a cohesion energy of -6.74 eV, compared to -6.81 eV for bcc molybdenum, which shows that the bcc structure is stable against fcc transformation.

To test numerical accuracy, two two-particle tests were performed. The first consists of two atoms starting outside each others sphere of influence, having 1 eV kinetic energy each. The velocities are directed toward each other, so the atoms perform a central collision. The deviation of the velocity ratio v_{before}/v_{after} from unity is a measure of inaccuracy. During the collision the atoms are inside each others cut-off range for exactly 100 steps and the velocity ratio turned out to be 0.999983. The second test was an oscillator test. Two atoms without kinetic energy are placed inside each others cut-off range. Their total energy after a little under 300 oscillations (some 10000 steps) is 0.93 times their starting potential energy. Compared to some of the approximations and assumptions made (applying Newtonian mechanics to solid state physics, neglecting angular dependence in the electron density, and using a numerical algorithm in an unstable system), the inaccuracy is acceptable, although certainly not small.

4.2 Surface relaxation

Free surfaces can be regarded as very large defects. One clearly noticeable effect of such a defect is surface relaxation of the first few planes near the surface. For a system based only on pair potentials this phenomenon is easily explained in fig. 9.
In EAM simulations the situation is more complicated. Omitting the embedding interaction would result in a lattice constant based purely on pair potentials, omitting the pair potential would result in a *different* lattice constant based only on the electron density. In EAM simulations the lattice constant lies somewhere in between. When a perfect crystal is cut in

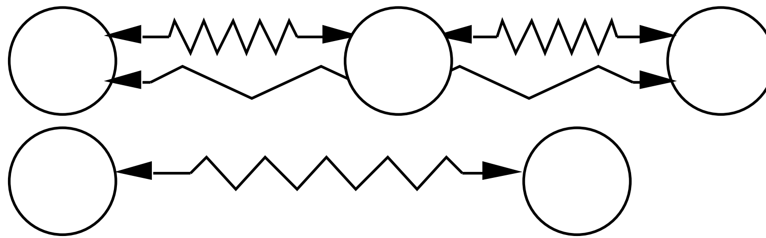

Figure 9. Increasing interatomic distance as a result of removing a neighbouring third atom. The pair of atoms shows the equilibrium distance for an isolated system of two atoms. The three interacting atoms show the decreased equilibrium distance when a third atom is added to the system due to next-nearest neighbour interactions.

two, the electron density varies, from high values far away from the free surface to low values at the surface. Depending on this density, the change in lattice constant may be an expansion or a contraction, because sometimes the effect of ‘cutting’ pair potentials may dominate (increasing the interatomic distances) and sometimes the decrease in electron density may dominate (decreasing the distance between atoms through the embedding interaction). The overall change is usually a contraction. The changes in lattice constant can be considerable. Figs. 10 to 12 show the lattice constant for planes near the surface of perfectly flat (100), (110), and (111) surfaces, obtained from the simulations.

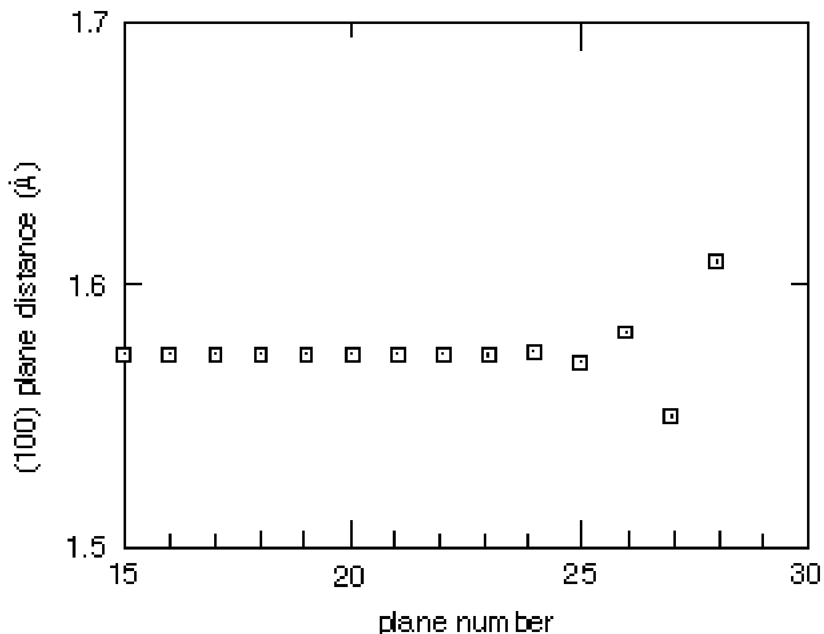

Figure 10. Distance between consecutive planes of a (100) surface after relaxation. The surface is at plane number 28. The bulk value is 1.5736 Å. In the simulations each atomic plane contains 196 atoms.

From figs. 10 to 12 it will be clear that near a surface, atoms are not located at regular distances. Also, diffusion of an atom over a surface can change the equilibrium position of other atoms. Locally, changes of up to 30 percent of the nearest neighbour distance have been observed in simulations.

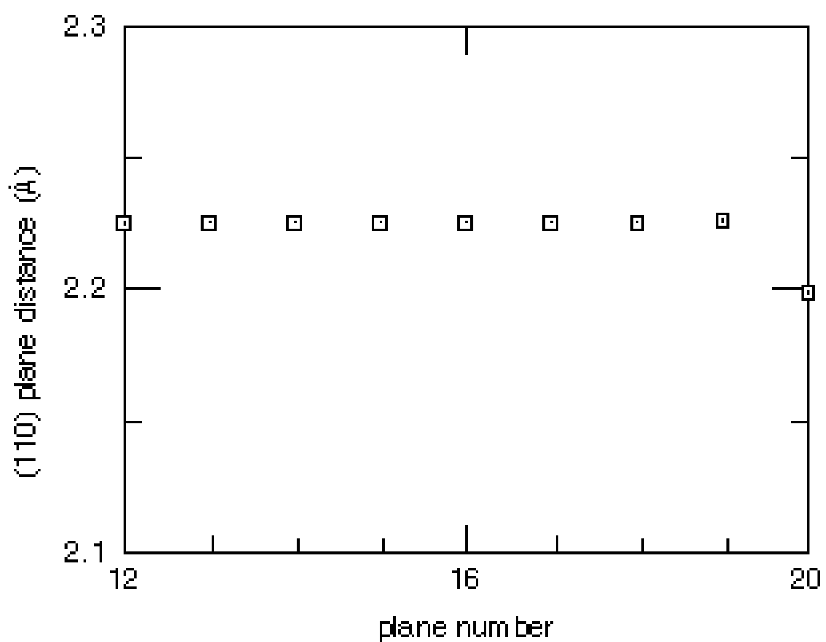

Figure 11. Distance between consecutive planes of a (110) surface after relaxation. The surface is at plane number 20. The bulk value is 2.2254 Å. In the simulations each atomic plane contains 280 atoms.

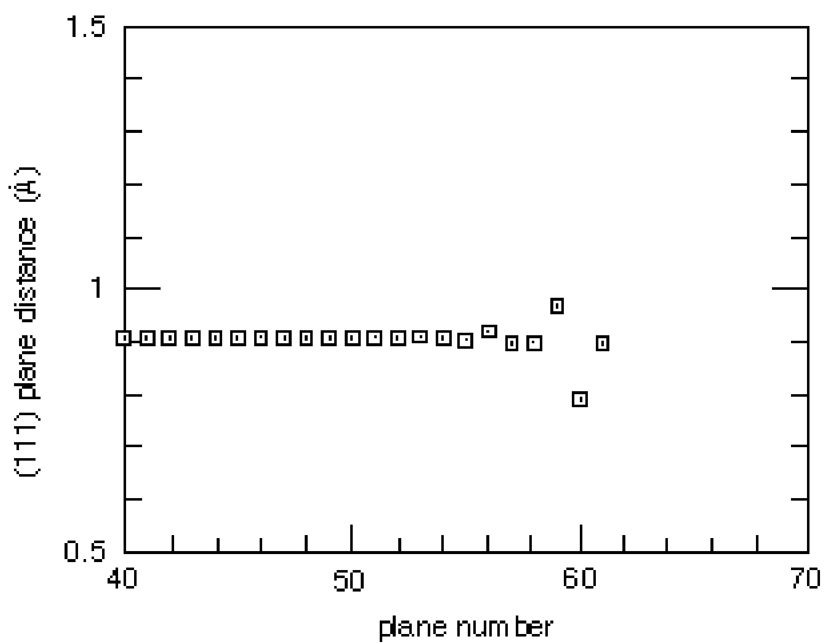

Figure 12. Distance between consecutive planes of a (111) surface after relaxation. The surface is at plane number 61. The bulk value is 0.9085Å. In the simulations each atomic plane contains 80 atoms.

The results above do not all agree with results reported by others. Zeper [12] and Robbemond and Thijsse [11] found contractions of 2.7 and 2.5 % in the distance between the first and second atomic planes of the (100) surface and 1.5 and 1.0 % contractions between the first and second atomic planes of the (110) surface. In the simulations in this thesis the distance between the first two planes of the (100) surface expands 2.2 % and the distance between the first two (110) planes contracts 1.1 %. The experimental value determined by Clarke [13], using LEED, for the (100) surface was a 9.5 % contraction. Clarke mentions that experimental results may be contradictory. For example, for the W (100) surface four LEED experiments resulted in contractions of 4.5, 5, 6, and 11 %. Ion scattering never resulted in a values higher than 6 %. Taking into account that all methods produce different results (even experiments using the same method and simulations using the same potentials), it should be concluded that the reliability of the results presented above is very limited.

4.3 Depositing films

The starting substrates for deposition runs are perfectly flat crystals. They usually consist of two atomic planes of bottom atoms with six or eight perfect planes on top to suppress any physically unrealistic influence of the bottom atoms. Most substrates were not relaxed before deposition. This was omitted because the time it takes the first atoms to reach the surface is long enough to allow for relaxation. Also, because the first few atoms on a large flat plane are usually too far separated to interact, the state of the surface at the beginning of the simulation is of little importance.

As a reference for the rest of section 4.3, table IV has been included. Here the deposition conditions and the main results of the simulations are listed.

4.3.1 PVD films

Earlier work has shown that different surface orientations develop distinctly different surface roughness characteristics. Using the Finnis-Sinclair EAM method, Robbemond and Thijsse [12] have shown for very thin films that (100) surfaces are relatively flat compared to (110) surfaces. To investigate this phenomenon further, a number of simulations have been calculated in which thicker films were deposited on (100) and (110) surfaces. Atoms were deposited at room temperature along the experimental 15/13° direction and with a 5.10^9 times higher deposition rate, see chapter 3. Results of simulations obtained under other conditions will be discussed in section 4.3.2 and beyond.

The results concerning the difference in surface roughness calculated with the Johnson-Oh EAM potentials are in agreement with the Finnis-Sinclair simulations by Robbemond and Thijsse. The Johnson-Oh simulations also show a rough (110) surface* and an almost flat (100) surface for thin films, see fig. 13. Figure 17 (ahead) shows the evolution of surface roughness for the first boxes of a number of films. After continued deposition up to 70 Å, using the ‘cut and shift down’ method (see chapter 3), the (100) surface still remains almost flat, but the (110) surface continues to roughen and this continued roughening eventually results in a columnar structure, see fig. 14.*

---

* Section 4.3.5 describes an attempt to explain surface roughness in terms of activation energies for migration.

* Interactive 3D impressions of a (110) film after deposition of the first and second box can be viewed in the files 1028box1.mcm and 1028box2.mcm. Interactive 3D impressions of a (100) film after deposition of the first and second box can be viewed in the files 1031box1.mcm and 1031box2.mcm.

Table IV. Data for the deposition runs. The surface orientation, the Ion to Atom Ratio, the argon energy, the molybdenum angle of incidence, the time interval between the deposition of two molybdenum atoms, the number of molybdenum atoms introduced during deposition, the total number of vacancies and vacancies in clusters introduced during deposition, the number of trapped argon ions (excluding those loosely trapped between columns, because these would have had time to diffuse away from between the columns in a real experiment), the number of sputtered molybdenum atoms, and the number of self-interstitials created during deposition.

MD run number	orien-tation	IAR	argon energy (eV)	Mo angle of incidence (°)	Mo dep. interv. (ps)	# of Mo introd.	# of vac-anc.****	# of trap. Ar	# of Mo sputtered	# of self-interst.
469 box 1*	(100)	PVD	-	normal	0.709	4038	39	-	0	0
469 box 2	(100)	PVD	-	normal	0.709	4086	130-140	-	0	0
468 box 1	(100)	PVD	-	30/0	0.709	3737	30	-	0	0
468 box 2	(100)	PVD	-	30/0	0.709	3906	140-150	-	0	0
1031 box 1	(100)	PVD	-	15/13	1.418	3985	40-50	-	0	0
1031 box 2	(100)	PVD	-	15/13	1.418	4560	40-50	-	0	0
1030 box 1	(100)	PVD	-	normal	1.418	4130	20	-	0	0
1030 box 2	(100)	PVD	-	normal	1.418	4495	100	-	0	0
1001	(100)	0.1	25/250 ***	normal	0.709	2800	9	3	32	2
1013 box 1	(100)	0.1	100/250	15/13	1.418	4155	4	3	no info.	6
1013 box 2	(100)	0.1	100/250	15/13	1.418	4045	5	3	no info.	4
484	(100)	0.1	250 (100x)	(sputtering)	-	-	6	8	63	no info.
1028 box 1	(110)	PVD	-	15/13	1.418	2966	19	-	0	0
1028 box 2	(110)	PVD	-	15/13	1.418	2195	7	-	0	0
1037**	(110)	PVD	-	15/13	1.418			-	0	0
1026 box 1	(110)	0.2	100	15/13	1.418	3474	3	2	102	12 *****
1026 box 2	(110)	0.2	100	15/13	1.418	2680	4	0	86	4
1003	(110)	0.1	25/250	15/13	1.418	3196	19	3	31	2
1020	(110)	0.1	100/250	15/13	1.418	3434	5	3	no info.	6
1007 box 1	(110)	0.1	100/250	15/13	1.418	3197	no info.	no info.	no info.	no info.
1007 box 2	(110)	0.1	100/250	15/13	1.418	2923	no info.	no info.	no info.	no info.
1034	(110)	0.2	100	normal	1.418	3440	3	0	106	10

* box 1 is the part of the film grown before cutting and shifting the film (see section 2.3.1), box 2 is the part grown afte cutting and shifting down

** film temperature was held at 2000 K

*** E/250 means that the argon energy was E but that 10 % of the ions had 250 eV kinetic energy

**** This is the total of 'empty' vacancies and vacancies containing Ar

***** 2 separately located interstitials and about 10 clustered in a small interstitial plane

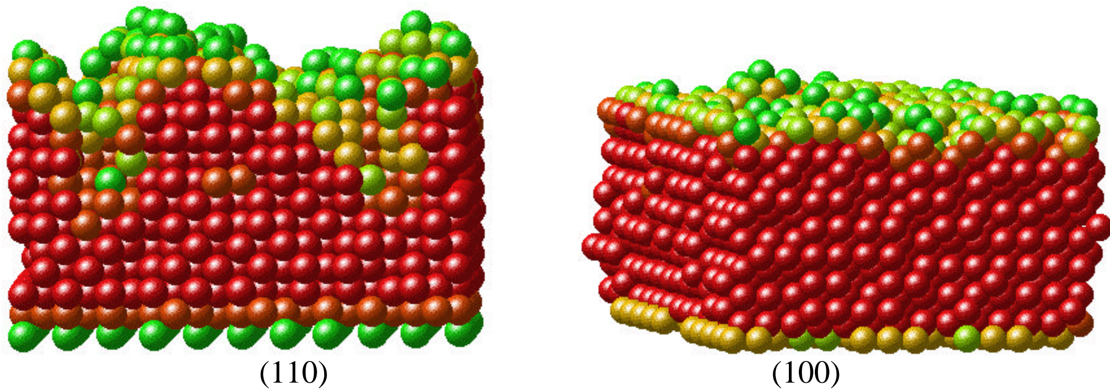

Figure 13. Thin films with (110) and (100) orientation. Colours indicate potential energy.

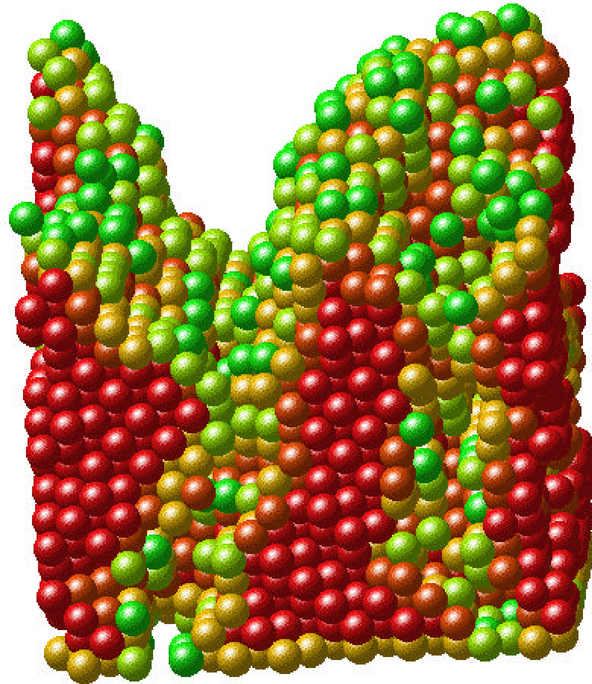

Figure 14. Upper part of a (110) film after 60 Å of nominal deposition. Colours indicate potential energy.

As can been seen from fig. 14 the surface contains a wave-like pattern which is a shadowing effect of the 15° off-normal deposition angle (normally deposited films do not show a wave-like pattern, see also section 4.3.3). No clear effect can be seen from the 13° angle with the (100) axis. This is probably because this effect (if there is any) is suppressed by the periodic boundary conditions. The wavelength of one 'wave' is about 20 Å, but this number may also be strongly determined by the periodic boundary conditions.

The columns grow from small protrusions. At first these appear insignificant, but because they stick out a little they attract slightly more atoms than the lower parts of the surface, because atoms 'stick' to the top and sides of these protrusions. This enlarges the protrusion slightly, making the lower parts of the surface even harder to reach. This process continues until the lower parts are completely sealed off from the incoming atoms. On the (100) surface no columnar structure develops, even after deposition of 70 Å. Small protrusions do develop, but the edges of these protrusions reconnect after continued deposition to form a flat surface again, incorporating the unoccupied lower lattice positions as vacancies and vacancy clusters, see fig. 15, instead of developing columns with open boundaries. This explains why the upper parts of thick (100) films have a higher vacancy concentration than the upper parts of (110) films. As yet, it is not fully understood why surface reconnection ('capping') prevails on (100) surfaces, whereas protrusion growth ('columns') prevails on (110) surfaces. There is no doubt however, that these effects are also responsible for the difference in surface roughness, as will be shown in fig. 17.

Together the first one or two planes of both the (100) and (110) films contain only 0-2 vacancies. As the deposition progresses, however, more and more vacancies and vacancy clusters are included, and after about 20 Å clusters of up to 10 vacancies[**] start to appear in the (100) film. The maximum cluster size in the (110) film is five vacancies. The defect concentration is much higher than the experimental value of $10^{-4}/10^{-5}$ [14], i.e. about one percent for the (100) film and about half a percent for the (110) films. After 40 Å the films were cut and shifted down and the deposition was continued. The second part of the

[**] Such large clusters are a rare event. By far most vacancies are included as single vacancies or bi- or tri

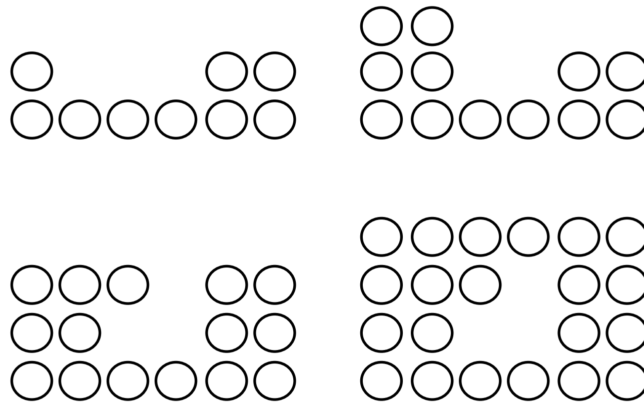

Figure 15. Schematic representation of the inclusion of a vacancy cluster on a (100) surface. Clusters are included on (100) surfaces because the edges around a developing cluster reconnect and seal off the unoccupied lattice sites.

(100) film contains as many vacancies as the first, with a smaller maximum cluster size of five vacancies. The (110) film contains far fewer vacancies (1/3 of the first box) and no clusters at all. This is probably because on (110) films the incoming atoms become attached to the tips of columns (once they have formed) and do not seal off unoccupied lattice positions as on (100) surfaces, instead leaving open the boundaries between columns. Neither the (100) nor the (110) films contain any self-interstitials. This is what one would expect.

The high vacancy concentration is the result of the high deposition speed. During the simulation there is no time for atoms to diffuse into surface vacancies, which therefore remain unoccupied and have been observed to turn into bulk vacancies after continued deposition, see fig. 15. The influence of the high deposition rate is confirmed by runs calculated at higher temperature, see also section 4.3.4.

Using the Finnis-Sinclair EAM potential, a thin (111) film has been deposited. It is too thin to obtain accurate information about the vacancy concentration, but it does show that the (111) surface develops a rough surface, see fig. 16.

All three surfaces contain weakly bound, low-coordinated atoms that ‘stick out’. This, too, is a result of the limited diffusion time because of the high deposition rate. The presence of such low-coordinated atoms, limited diffusion time, and possible implications for the appearance of the columnar structures are discussed in sections 4.3.4 and 4.5.1.

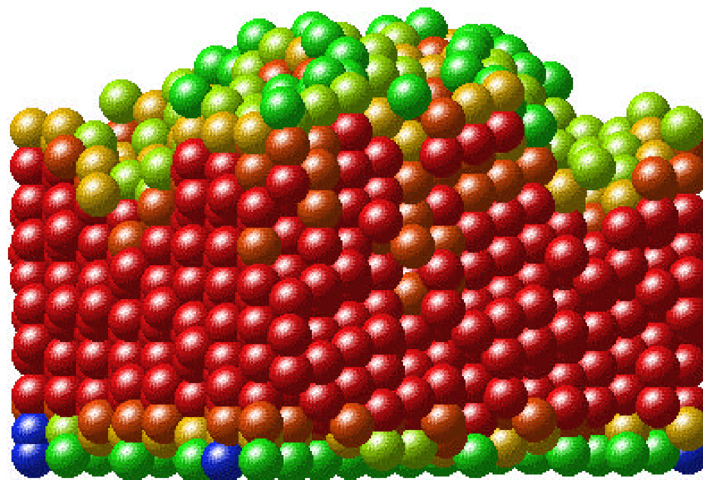

Figure 16. Thin (111) film. Colours indicate potential energy.*

vacancy clusters.

* A 3D impression can be viewed in the file 111film.mcm

4.3.2 Influence of argon ions on vacancies and surface roughness

A number of films have been deposited with 25 or 100 eV argon ion assistance. The IAR was 0.1, except in one simulation with 100 eV ions, in which the IAR was 0.2. Most beams were contaminated with 10 percent 250 eV ions.

The ion assistance has a very clear flattening effect on films, both delaying the onset of columnar growth and decreasing the width of the boundaries between columns. The delay in the onset of columnar growth can been seen in fig. 17. This figure shows the film roughness (defined as the standard deviation of the height of all surface atoms. Atoms are considered surface atoms when they have the same or fewer nearest and next-nearest neighbours than an atom in a perfect flat surface, i.e. 9 for (100) surfaces and 10 for (110) surfaces.) as a function of the nominal film thickness for five films. The ion energy input for these films varies from none (PVD) to 100 eV ions with an IAR of 0.2.

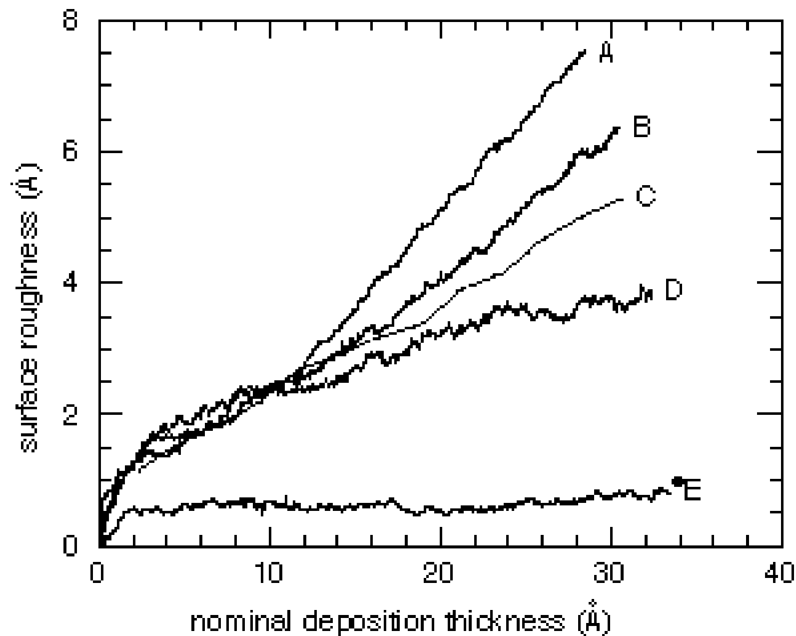

Figure 17. The surface roughness as a function of nominal film thickness. The curve A corresponds to an unassisted (110) film, curve B corresponds to a (110) film assisted with 25 eV ions, contaminated with 10 percent 250 eV ions, curve C corresponds to a (110) film assisted with 100 eV ions, contaminated with 10 percent 250 eV ions, curve D corresponds to a (110) film assisted with 100 eV ions without contamination, and curve E corresponds to a (100) film assisted with 100 eV ions with 10 percent 250 eV contamination. The IAR for curves B, C and E is 0.1 and the IAR for curve D is 0.2.* The dot corresponds to the roughness of a PVD (100) film after 34 Å of nominal deposition (the full curve is not available).

* Interactive 3D impressions of the last configurations of the first and second box of the deposition run corresponding to curve B can be viewed in the files 1003box1.mcm and 1003box2.mcm. An interactive 3D impression of the last configuration of the first box of the deposition run corresponding to curve C can be viewed in the file 1020.mcm. The growing of the second box of a film with deposition conditions similar to those of run 1020 can be viewed in the movie (110) columns.mov. Interactive 3D impressions of the last configurations of the first and second box of the deposition run corresponding to curve D can be viewed in the files 1026box1.mcm and 1026box2.mcm.

It can be seen from figure 17 that a certain minimum roughness (a standard deviation of about one monolayer) is required for the argon ions to have any effect, as it is very difficult to make an almost flat surface even flatter. The point where al four curves intersect does not appear to have any special relevance. Fig. 18 shows two films, one deposited without ion assistance and one assisted with 100 eV ions and an IAR of 0.2. The figure shows that the ions delay the onset of columnar growth (this effect was not noticed for 100 eV by Robbemond and Thijsse, probably because of the limited thickness of the deposited films.). Unfortunately, it is not possible to determine surface roughness from TDS spectra, so comparison between the simulations and these experiments is not possible. However, the flattening effects seems realistic enough.

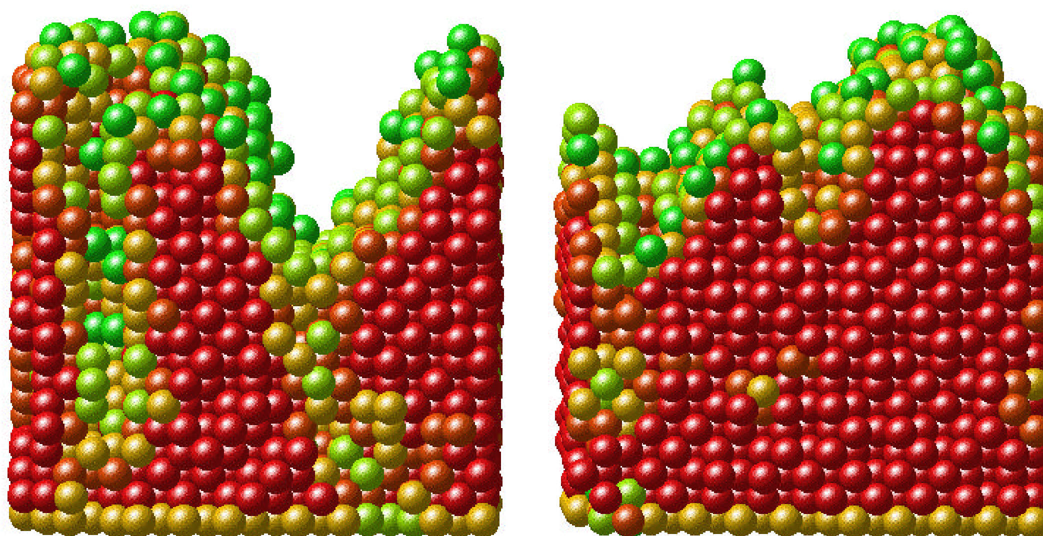

Figure 18. Films deposited on (110) substrates. The left film was deposited without ion assistance, the right film was assisted with 100 eV ions and an IAR of 0.2. Colours indicate potential energy.

The ion assistance also affects the number* (see later this section) and types of defects in the film. This influence is limited to a very thin surface layer, but of course this surface layer moves along with the growing film. To investigate the maximum depth up to which argon ions influence films, a series of 150 short simulations has been calculated, each one consisting of one 250 eV argon impact on the same (110) surface with columnar structures. The starting points of the incident trajectories were varied randomly. The positions of the ions where they have penetrated deepest into the film are registered. A second simulation consisted of one series of 100 consecutive 250 eV impacts on a flat (as flat as the film shown in fig. 13) thin (100) film. From this simulation only the final positions of the argon atoms that remain trapped are known. Further results were obtained by examining the 250 eV ions in contaminated 25 and 100 eV beams. Because of the limited number of argon ions involved (no more than a few thousand in all simulations together, hardly ever more than a hundred in one specific simulation) the inaccuracy may be quite large.

The results for 250 eV argon ions show that most ions are deflected by the first or second plane. Trapping hardly ever occurs in the first planes. A small number of ions penetrate into the third and fourth plane, hardly ever any deeper, see fig 19. The ions that penetrate though the first few planes have a very large probability of becoming trapped. The total trapping probabilities of 250 eV ions are about 8 % for the both the (100) and the (110) surface. Trapping of ions usually takes place after the argon ion has displaced one or more molybdenum atoms from their lattice positions, creating monovacancies or vacancy clusters of up to four vacancies, in which the ion itself remains trapped. The displaced molybdenum atoms often set so-called replacement collision sequences (RCSs) into motion, in which

* Numbers of defects and defect concentrations always apply to the entire box except for the bottom atoms, unless mentioned otherwise.

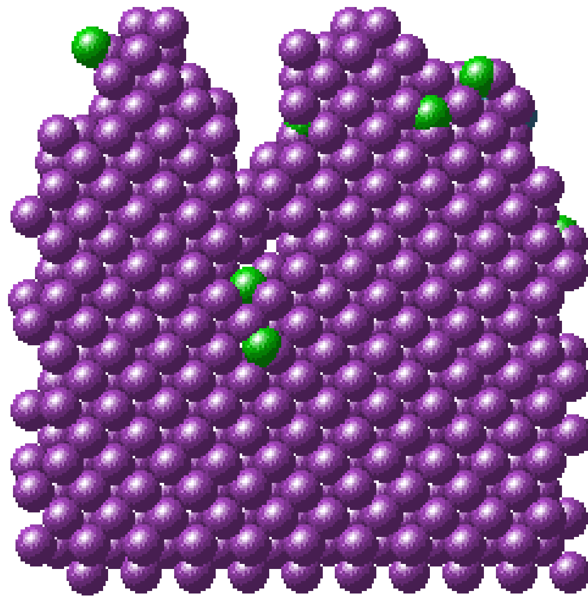

Figure 19: Film cross section showing the maximum penetration depths of a few 250 eV Ar ions (green) in a (110) film.*

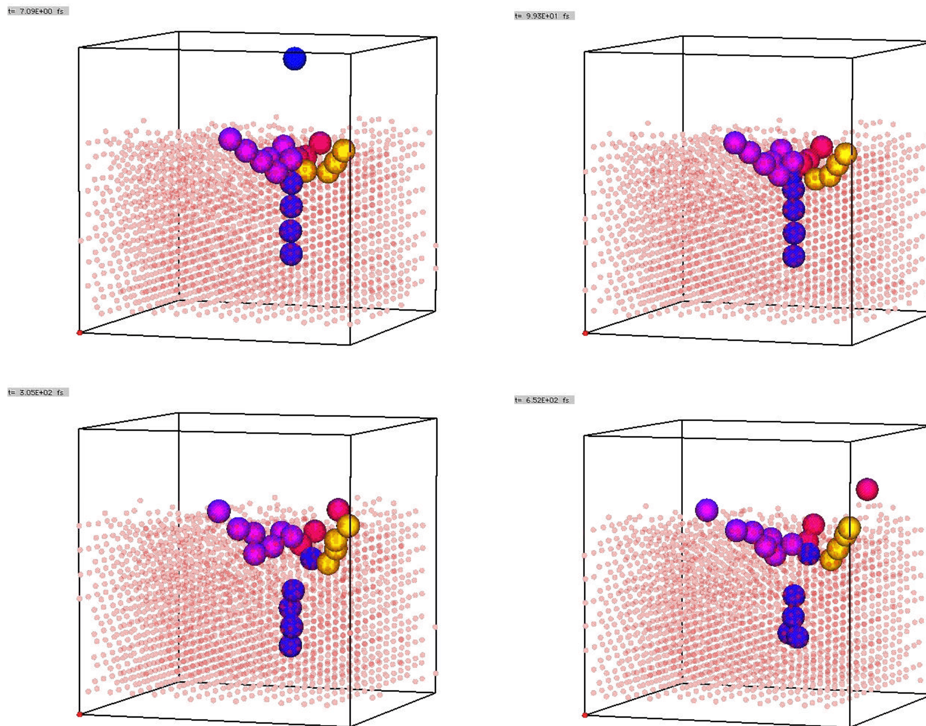

Figure 20. Impact of a 250 eV argon ion. The ion (blue) penetrates the first three atomic planes, after which collisions with four atoms result in four replacement collisions. Three lead to the surface, the fourth results in the creation of a self-interstitial (the dumbbell in the lower part of the fourth picture). The ion itself remains trapped in the cluster it created (separate blue particle).*

---

* The starting configuration with all the minimum height positions in it can be viewed in the file 1025.mcm.

* The full animation from which these pictures were taken can be viewed in the file replacementcol.mov.

they act as the trailing atoms. Most RCSs (about two thirds) lead to the surface. It is possible for the head atom in a RCS leading to the surface to move several positions over the surface, disconnecting itself from the rest of the RCS. RCSs that are pointed downward can end up in other vacancies or clusters, or create self-interstitials. The first effect takes place only in films that contain many vacancies, because the RCS lengths are too short to have an appreciable probability of reaching a vacancy in films with low vacancy concentrations. RCSs of up to 14 atoms occur, but the average length is just 4.1 atoms. Figure 20 shows a few pictures from an argon impact that results in the creation of a cluster of four vacancies in which the argon ion itself remains trapped. Three of the four molybdenum atoms are removed by replacement collisions leading to the surface, the fourth is removed by a replacement collision that results in the creation of a self-interstitial.

Apart from initiating RCSs, argon ions can pass energy to the lattice by local melting. During local melting the energy of the ion is not passed to a select number of atoms that transfer the energy away from the place of impact through RCSs, instead all atoms in an area close to the impact gain so much energy that the crystal structure is temporarily destroyed, see fig. 21.

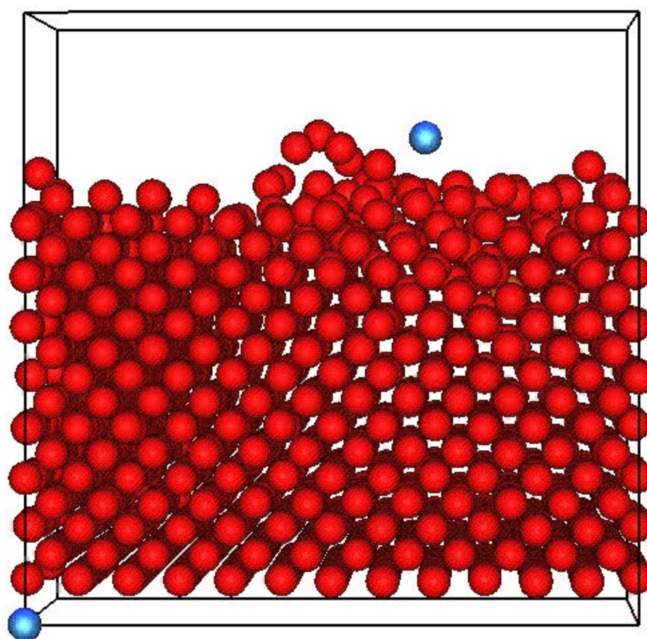

Figure 21. Surface of a (100) film 0.5 ps after a 250 eV argon ion (blue) has hit the surface. The blue particle in the bottom of the picture has no significance.[**]

A small number of ions is trapped in existing vacancies or interstitial positions. Interstitial trappings are a rare event (approximately one out of every 10 trapped ions traps as an interstitial) which increases the lattice energy by 13.3 eV, much more than the substitutional energy increase of 2.8 eV. Substitutionally trapped argon increases the distance of its nearest neighbours by 1 percent.

Argon atoms that are only deflected and subsequently backscattered still have a significant effect on the film. They can create self-interstitials and displace or remove molybdenum atoms or locally melt the surface. They can also cause previously trapped argon atoms to desorb[*] . On columnar (110) surfaces the sputter coefficient for 250 eV argon is 0.46, on flat (100) surfaces it is 0.63. The value of 0.46 is in good agreement with the empirical value of 0.47 found (no surface orientation was mentioned) by Bohdansky *et al* [15]. The higher value for (100) surfaces is due to the fact that there are no columnar

[**] The full animation from which these pictures were taken can be viewed in the file localmelt.mov.

[*] An animation of such an event in which a 250 eV argon ion desorbs a previously trapped argon ion can be viewed in the file desorb.mov.

structures which can block a free atoms path away from the surface as is the case on (110) surfaces.

On average 20 molybdenum atoms are displaced by one or more lattice positions in a (110) film by a 250 eV ion impact, 11 atoms lose so many neighbours that they become surface atoms, and 10 atoms gain so many neighbours that they become bulk atoms. The number of neighbours of all atoms that are moved by an ion impact increases from 7.2 to 8.1, showing that on average the atoms move into more stable positions. This is the explanation for the flattening of surfaces and the decrease in the high number of vacancies and vacancy clusters that would have appeared without ion assistance: weakly bound, low-coordinated atoms move into more stable positions (like surface vacancies), reducing the protrusions and filling potential vacancies.

The effects of 100 eV argon ions are less pronounced than 250 eV argon effects: fewer RCSs occur, creation of clusters is never observed, the sputtercoefficient on (110) surfaces is 0.14 (in agreement with the orientation-independent value of 0.13 by Bohdansky), and the trapping is much lower, 0.3 percent. The number of displaced molybdenum atoms is still considerable, 10 on average (although this value is lower than the value of 20 found by Robbemond and Thijsse, a difference which can only be ascribed to the differences between Johnson-Oh and Finnis-Sinclair EAM potentials, since in both simulations the ions impinged perpendicular to the surface), which explains the lowest (110) curve in fig. 17. Despite the lower number of RCSs, self-interstitials are still created by 100 eV argon ions. During the deposition of a film assisted with 100 eV ions and an IAR of 0.2, 12 self-interstitials were found after 1208 ion impacts. The self-interstitial creation yield is probably higher than 0.01 because self-interstitials are very mobile, even at low temperatures (see also section 4.5.2), and many self-interstitials will have been removed from the film by the ion bombardment. How many is not known. The interstitials that were observed in the film were first concentrated in a small part of the film as separate interstitials. The concentration in a small part of the film appeared coincidental. Near the interstitials the planes were bended in a chaotic way at first. After continued deposition the interstitials clustered together and formed two dislocations, their half-planes having a small overlap, thus accommodating the extra atoms, see fig. 22. The half-plane overlap never was more than two atoms long. It should be noted that self-interstitials are very mobile in real experiments and that it is very well possible that the interstitial plane would not have appeared in a real experiment because diffusion would have diluted the self-interstitial concentration. Also, the periodic boundary conditions parallel to the surface force the planes to bend in less than 50 Å, a very small distance for dislocations. Although the mechanism of an interstitial plane to accommodate interstitials is known to exist, the length over which the planes are bended is very unrealistic.

The effects of 25 eV argon are marginal. No trapping or sputtering takes place[**] and on average only two molybdenum atoms are displaced.[***]

The effects of argon ions on the defect concentration are not easily compared to experiments, because experimental PVD films contain very low numbers of vacancies and therefore argon ions will often create more defects than they can remove. In simulations the ion bombardment always results in a decrease in defect concentration. In 30 Å deposition experiments on a (100) single crystal with 250 and 100 eV (IAR = 0.1) uncontaminated IBAD the concentration of vacancies and argon filled vacancies increases to $1*10^{-3}$ and $4*10^{-4}$, up from $3*10^{-5}$ for PVD experiments. In MD simulations the vacancy concentration in 250 eV contaminated 100 eV argon IBAD runs decreases from $2*10^{-2}$ to $6*10^{-4}$ and in a simulation with pure 100 eV ions and an IAR of 0.2, the vacancy concentration is $9*10^{-4}$.

The MD vacancy concentration for 100 eV ion assistance with an IAR of 0.2 is about twice the concentration found in the experiment with an IAR of 0.1. Assuming that

---

[**] In some cases a 25 eV ion was trapped between two columns after which the newly deposited molybdenum atoms closed off the boundary. This trapping is due to the high deposition rate because in reality the argon atom would have had plenty of time to escape. Therefore these trappings are not included in any calculations.

[***] An animation showing 8 impacts of 25 eV ions on a (100) surface can be viewed in the file 25eVs.mov

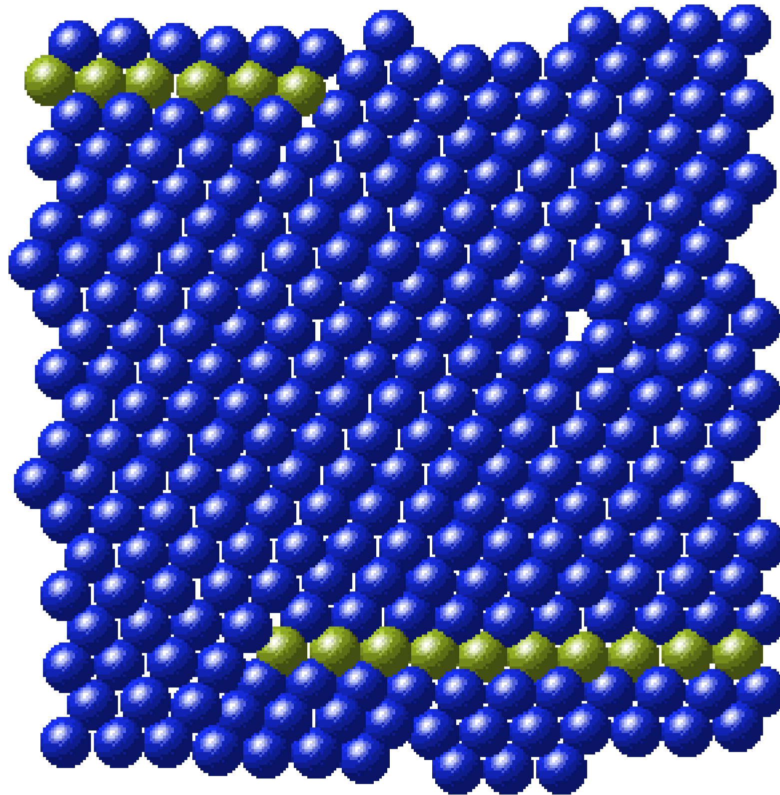

Figure 22. Top view representation of interstitial accommodation by creation of two dislocations with slightly overlapping half-planes.*

(starting from a perfect, defect-free crystal) the vacancy concentration is proportional to the IAR for low concentrations, these results are in good agreement. Unfortunately, there are no pure 250 eV deposition simulations.
Still, a rough comparison between experiments and the 100 eV simulation with 10 percent 250 eV contamination can be made by assuming that in experiments the effects of 100 and 250 eV ions are independent (an admittedly doubtful assumption). In that case the defect concentration should be $0.1*1*10^{-3} + 0.9*4*10^{-4} = 4.6*10^{-4}$. This value lies close to the value of $6*10^{-4}$ found in the simulation. It should be noted that the number of vacancies in IBAD simulations is very small (see table IV) and that the defect concentration is therefore very sensitive to the exact number that happens to be found. Still, the numbers of vacancies in IBAD simulations agree reasonably well with experiments. The 250 eV argon trapping found in simulations and experiments (both 8 %) is also in agreement. The mechanism of cluster creation by replacement collisions can not be verified by TDS but more clusters are observed in IBAD spectra than in PVD spectra and RCSs seem a credible explanation.

4.3.3 Influence of the deposition angle on vacancies and surface roughness

Earlier work [11] has shown that a (110) film deposited with a 30° off-normal angle is rougher than a film deposited at normal incidence. To further investigate this phenomenon, a number of simulations with normal and 30° off-normal deposition angles have been calculated for comparison with the 15/13° angle.

* This figure was taken from the file 1026box1.mcm.

On (100) surfaces both the normally and the 30˚ off-normal deposited films, deposited without ion assistance, remained almost flat (a standard deviation of about one monolayer) during the deposition of the first 30 Å. Small variations in the molybdenum flux evened out, although vacancies and clusters were of course included in the film. After 30 Å a large holes started to appear in both simulations, apparently as the result of a fluctuation in the molybdenum flux. The protruding edges of this hole attracted other atoms, enlarging the edges, and making the lower part of the film more difficult to reach. This process continued until the edges were reconnected and the hole had been fully sealed off. The mechanism by which the large holes were created does not appear to be different from the mechanism by which momovacancies and small clusters are created, the flux variation appears to be the governing parameter. The hole found in film with a normal deposition angle consisted of some 50 vacancies, the hole in the 30˚ film consisted of some 40 vacancies. After the holes had been sealed off, the surface is only slightly rougher than at the time just before the hole appears, see fig 22. Fig. 22 shows various stages of the process described above.

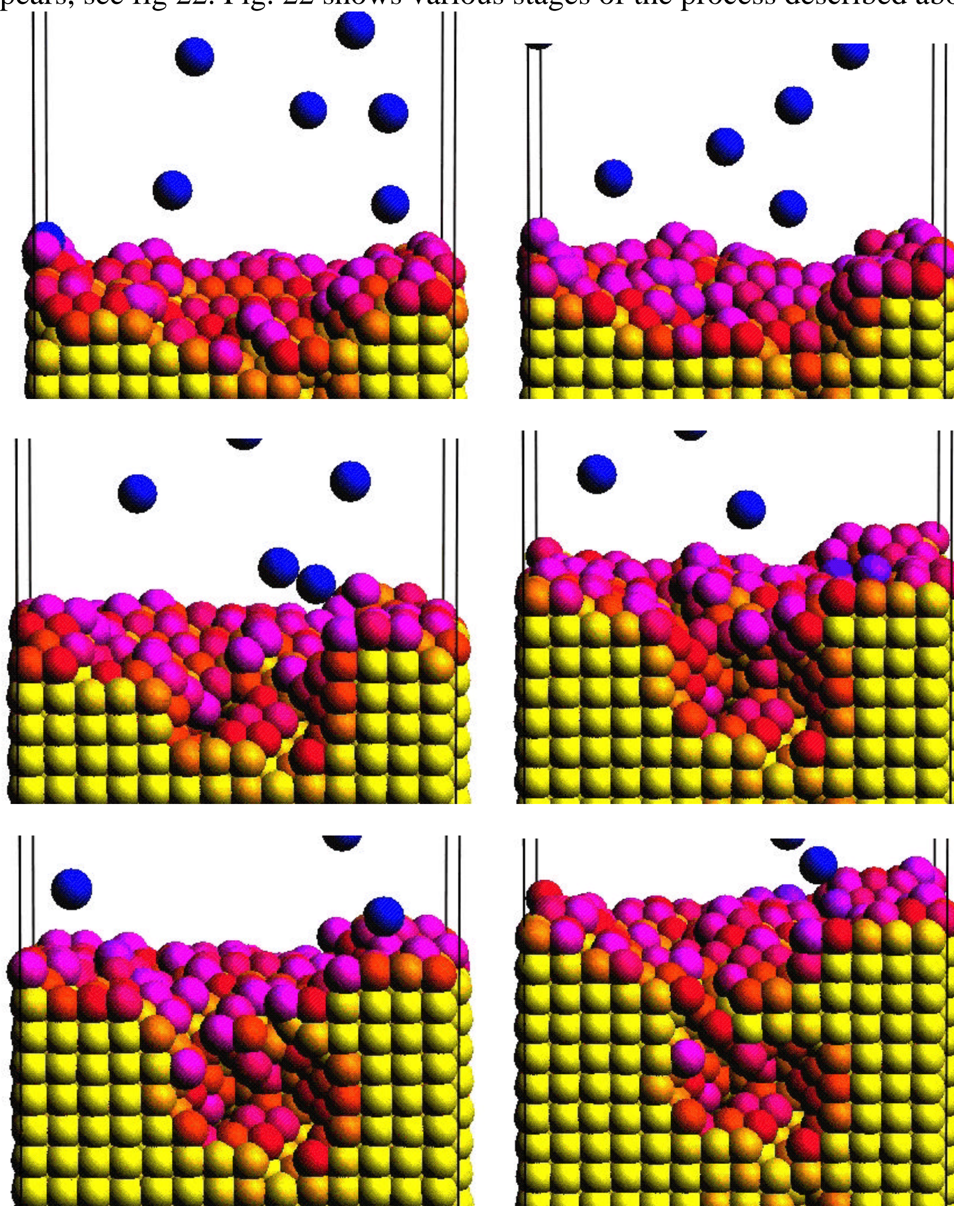

Figure 22. Various stages in the inclusion of a large hole, consisting of some 50 vacancies, that started to appear after 30 Å of nominal deposition thickness. The molybdenum atoms are deposited with normal incidence. Colours indicate potential energy.[*]

---

[*] The pictures in this figure were taken from the animation largehole.mov. The growing of the large hole

The holes are quite stable: 250 eV ions intentionally directed at the holes change their shape but do not cause their collapse.[**]

The large size of the holes is probably due to the high deposition rate. In a real experiment part of the fluctuation in the molybdenum flux can be compensated by surface diffusion. Deposition at higher temperatures or with ion assistance would probably decrease the hole size significantly. The angle dependence does not appear to be related to simulation conditions. When comparing the films deposited with normal and 30˚ angles, the 30˚ angle film does not have a significantly rougher surface than the normally deposited film, contradicting the findings on (110) surfaces by Robbemond and Thijsse. However, it should be noted that since the surfaces of both (100) films remain quite flat, it is difficult to draw any conclusions with certainty.

The concentration of vacancies in the normally and 30˚ off-normally deposited films are even higher (3 percent) than the concentration of vacancies found in films with a 15/13˚ deposition angle (2 percent). There is no clear explanation for this phenomenon.

Like the normally deposited (100) film, a normally deposited (110) IBAD film (IAR = 0.2, 100 eV) develops small height variations after the first few planes, and as in the 15/13˚ (110) case, these do not reconnect but form columnar structures. Contrary to the 15/13˚ case there is no wave-like pattern, columns are roughly rounded. Fig. 23 shows the surface roughness of the normally deposited (110) film and of a film with similar IBAD conditions but with 15˚ incidence. Fig. 24 shows the columns of the normally deposited film.

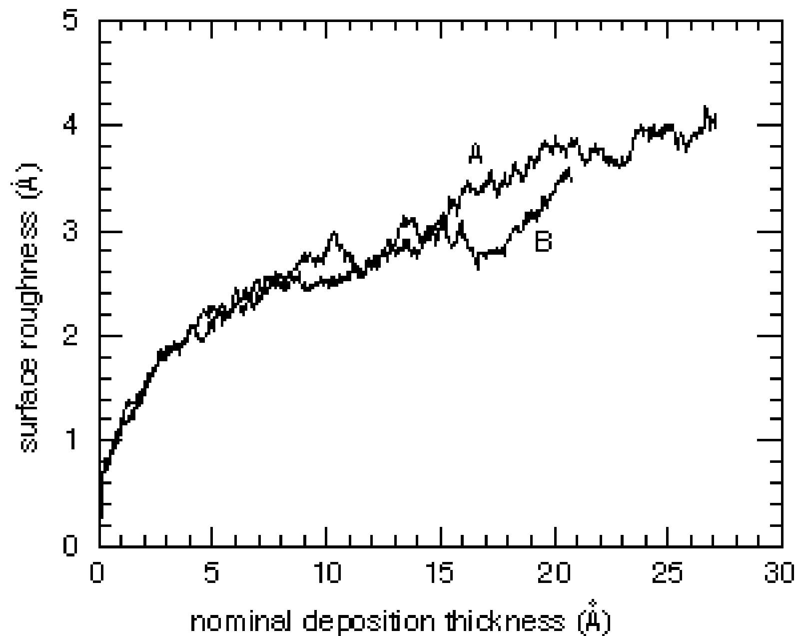

Figure 23. Surface roughness as a function of deposition thickness of two films, one with 15˚ incidence (A) and one with normal incidence (B).

It can be seen from figure 23 that the deposition angle has little effect on the roughness perpendicular to the film.

The number of vacancies in the (110) film is more or less equal to the number in the 15/13˚ deposited films, but this observation has only a small significance due to the very

---

in the film deposited with a 30˚ deposition angle is shown in the file largehole30.mov.

[**] some of these impacts (directed either central at atoms or at channeling directions) can be viewed in the files impacts1.mov, impact2.mov, and impact3.mov.

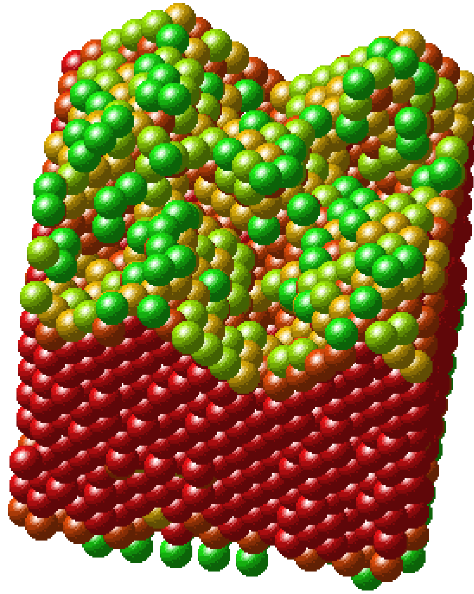

Figure 24. A normally deposited (110) IBAD film (100 eV, IAR = 0.2). Colours indicate potential energy.*

small number of vacancies on which it is based.

On the whole the results of the angle dependence are not very well understood. The wave-like pattern for (110) films with a 15/13° deposition angle is obvious, but there is no explanation for why (100) films with normal and 30° deposition angles incorporate holes of dozens of clusters and films with a 15/13° deposition angle do not.

4.3.4 Influence of the deposition rate and temperature

As mentioned in chapter 3 the deposition rate and temperature have both been varied to get a rough estimate of the influence of diffusion during deposition. Lowering the deposition rate by a factor of two was not expected to have a significant impact, because it will still be more than 10^9 times too high, and therefore almost all diffusion time is still left out of the simulation. Indeed no influence was found.

Raising the film temperature from 300 K to 2000 K has a much greater influence, because many more thermally activated atomic jumps will be able to take place. The factor by which the number of 'successful jumps' (atomic motions by which an atom moves to a different lattice position) increases, depends on the activation energy. For a low migration energy of 0.25 eV, typical for surface diffusion (see also section 4.3.5), the number of successful jumps increases by roughly 3500 times, for an activation energy of 1 eV the number increases by more than a factor of 10^{14}. Despite this, it is still only low-coordinated surface atoms that show any significant mobility, see also section 4.5.1.

One (110) film has been deposited without argon assistance at a film temperature of 2000 K. Fig. 25 shows the surface roughness compared to a PVD (110) film deposited at 300 K. It can be seen from fig 25 that raising the temperature to 2000 K only has a modest effect on the surface roughness. The influence of elevated temperature is smaller than the influence of 25 eV IBAD with 10 % 250 eV contamination, the lowest energy input of any IBAD deposition run in this thesis.

Raising the film temperature significantly reduces the defect concentration: the film grown at 300 K contained 12 vacancies in the first four planes after 7 planes had been nominally deposited. The film grown at 2000 K contained just two, confirming the conclusion in section 4.3.1 that the high number of vacancies in PVD film are the result of

---

* This figure was taken from the file 1034.mcm.

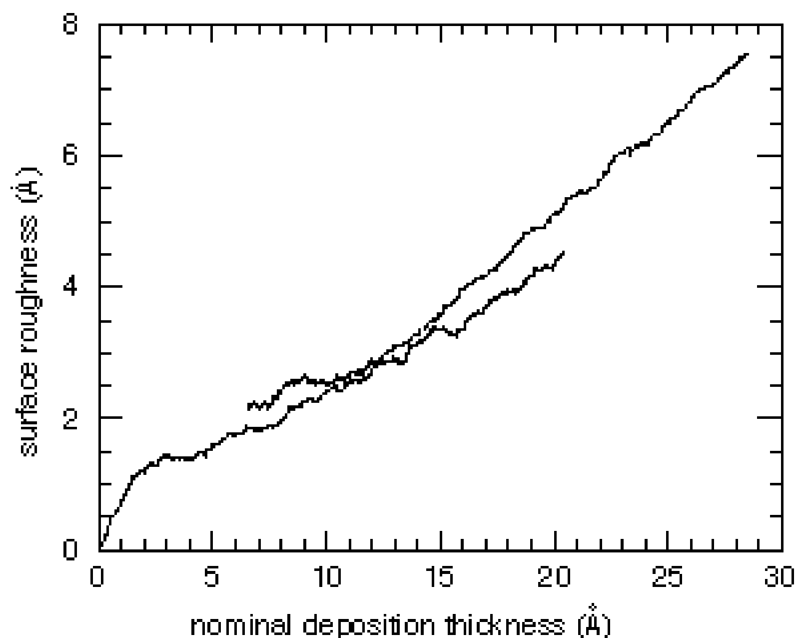

Figure 25. The surface roughness as a function of deposition thickness for a film deposited at 300 K (dashed curve) and 2000 K (full curve).

the high deposition rate. Although the figures mentioned above are determined from a simulation on a (110) surface, it is logical to conclude from this simulation that the large holes in normally deposited (100) films will be significantly smaller in real experiments or simulations carried out at 2000 K, because part of the fluctuations in the molybdenum flux will be compensated by the elevated temperature in much the same way as ion assistance flattens films and reduces the number of vacancies of simulated PVD films.

Both the reduced vacancy concentration and smoother surface found in the simulation are in agreement with the general expectations for a 2000 K deposited film. The results of further investigation into the effects of diffusion at high temperature are presented in section 4.5.

4.3.5 Surface roughness explained by activation energies

Robbemond and Thijsse 12 gave the difference in migration energies of single atoms on perfectly flat (100) and (110) surfaces as the explanation for the difference in roughness between (100) and (110) films. They proposed that (110) surfaces are rougher because atoms have to move over other planes with higher migration energies if they are to be struck down a hill by incoming ions. However, this explanation is invalid for surfaces consisting of many small, different surfaces.

To further investigate the difference between (100) and (110) surface roughness, an artificial landscape* as shown in fig. 26 was created.** It consists of a pyramid with a flat top. The horizontal planes are (100) planes, the other planes are (110) planes. A few atoms were placed on the flat surfaces and near the edges between the (100) and (110) planes. The original idea was to anneal this artificial substrate without depositing molybdenum or sputtering so that diffusion could be clearly studied, in the expectation that the pyramid

---

* See file 375.mcm for a 3D impression

** The Finnis-Sinclair EAM potential was used for calculating the results in this section

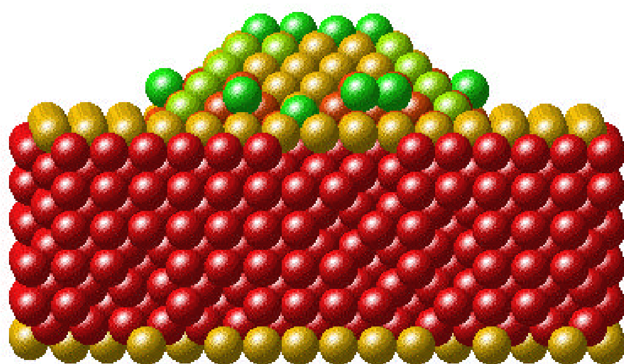

Figure 26. Substrate with a pyramid to study surface diffusion.
Colours indicate potential energy.

shrinked and the surface turned into a flat (100) surface. However, the pyramid did not disappear. The atoms that were placed on the flat surface and near the pyramid edges showed a clear preference to diffuse onto the top plane of the pyramid. After annealing for 0.8 ns at 600 K the pyramid top had grown a full plane. This unexpected result was reason to investigate the activation energies required to go from one plane to the other, using the 'cold' method described in chapter 3. The energy required for an atom on a flat surface to be pulled away from the surface and the migration energies found by Robbemond and Thijsse for the (100) and (110) planes were also recalculated. The results are presented in fig. 27.

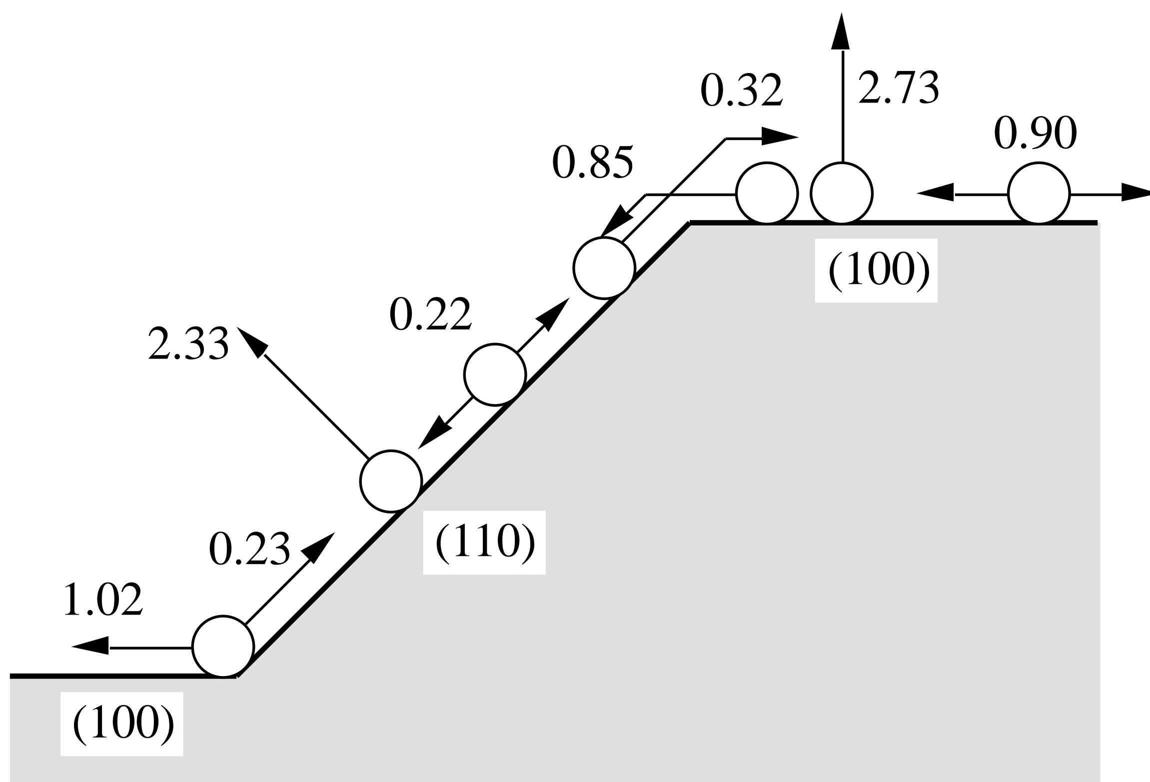

Figure 27. Activation energies in eV for a number of diffusion processes and desorption from (100) and (110) surfaces. These results were calculated with the Finnis-Sinclair EAM potential.

Note that when an atom completes the cycle / desorption from (100) / adsorption on (110) / migration from (110) to (100) / the net energy change is not equal to zero. This seeming violation of energy conservation is caused by the different amounts of kinetic energy absorbed by the lattice during different diffusion steps. When an atom moves from the (110) surface to the upper (100) surface it loses little energy to the lattice. When it moves back to the (110) surface it transfers more energy. The energy transferred to the lattice is the main reason of inaccuracy.

It can be seen from fig. 27 that at both edges the molybdenum atoms require less energy to move upwards than downwards. This explains why the pyramid top turned out to grow. Although the flat surface-plus-pyramid is an artificial situation, the results show that explaining differences in surface roughness by migration energies for flat surfaces is impossible. From fig. 14 it is clear that a real film surface consists of dozens of different surface orientations, each one consisting of only a few lattice positions, so dozens (maybe even hundreds) of activation energies play a role. This disproves the explanation by Robbemond and Thijsse. A working explanation to replace their explanation is not available. From the deposited films it can be concluded that the differences between (100) and (110) films are mainly due to the fact that on (100) films any protrusions reconnect whereas on (110) films they do not. This can not be explained by activation energies.

The energies in fig. 27 are determined using the 'cold' method described in chapter 3. In order to check the reliability of this method, a flat (110) film with a single atom on top was annealed at 400 K for 90 ps. The time average vibrational frequency of the adatom parallel to the surface is 4.6 THz*. From the number of vibrational period N and the number of observed jumps n the activation energy ΔE is calculated, using the very simple model

$$n = jNe^{-\frac{E}{kT}}, \tag{31}$$

in which k and T have their usual meaning. The factor j is the number of attempted jumps per vibrational period, for which a value of 2 was chosen in this case. This value only has a limited physical foundation, but because the factor jN is related to E as $E \sim \ln(jN)$, the actual value of j or N is not all that important. The activation energy was found to be 0.16 eV. This value is considered close enough to the previously determined value of 0.22 eV to conclude that the cold method produces reasonably accurate values compared to real diffusion. The value determined from diffusion has not been compared to experimental data. However, Papanicolaou *et al* [16] have shown for silver (100) and (111) surfaces that activation energies can be determined with reasonable accuracy by studying adatom diffusion in a MD simulation.

4.4 Helium decoration

In order to determine how deep helium ions penetrate films, 888 helium impacts on a grown (100) film have been calculated to determine an implantation profile (see also chapter 3). The film had a smooth surface, comparable to the (100) surface shown in fig. 13, and contained few defects, therefore trapping in existing defects can be ignored. The result is shown in fig. 28, along with TRIM-results [17] for the same conditions. In MD simulations the penetration depth was measured as the distance perpendicular to the film between the point where the ion first penetrates the surface and the point where the ion has penetrated deepest into the surface. TRIM calculations measure the distance between the point of penetration and the point where the kinetic energy of the ion has dropped below a certain value.

* This frequency was determined by registering the number of times the atom moves closer to and further away from its equilibrium position parallel to the surface and dividing this value by 2.

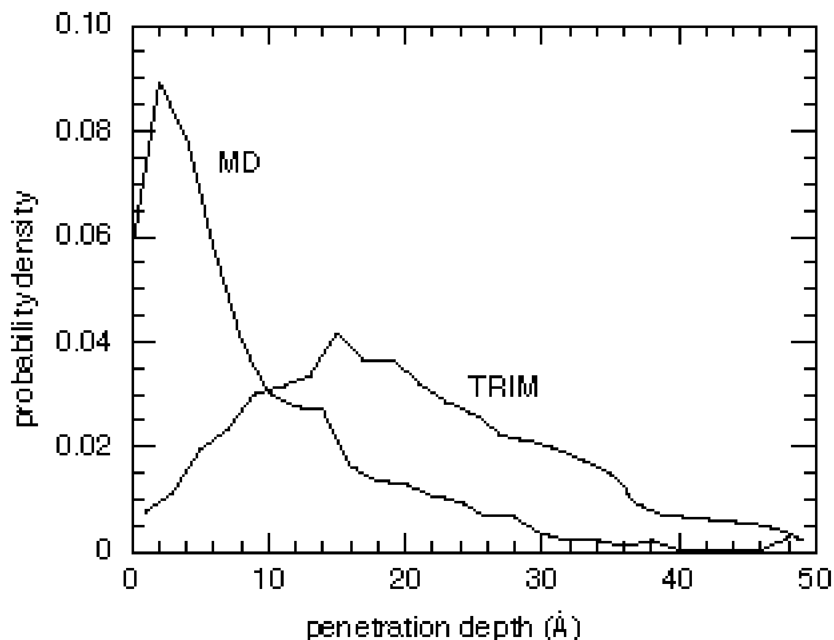

Figure 28. Implantation profile of 100 eV helium on a molybdenum (100) surface, determined from MD calculations and TRIM results. The angle of incidence is 20° off-normal, parallel to the <100> direction. The bottom atoms were located at 48 Å.

It can be seen from fig. 28 that the average penetration depth in MD simulations is about 8 Å and that hardly any ions penetrate deeper than 30 Å. Note that the TRIM results show a significantly greater penetration depth than the MD simulations. It should be noted that the TRIM results are based on a number of strong simplifications. The most important one for comparison of TRIM results with the MD implantation profile is the neglection of ions that penetrate the film and leave again. This means that a large fraction of ions in TDS experiments probe layers thinner than those predicted by TRIM.

Looking at xz- or yz-projections of the helium trajectories shows that the helium ions do not channel over any long distances. The helium ions are usually scattered before having passed through seven or eight planes. Because of the short velocity auto-correlation length, implantation profiles for films with different orientations are not expected to differ greatly from fig. 28, except if the orientation is chosen in such a way that a channeling direction lies within a few degrees of the angle of incidence. Two examples of helium trajectory projections, one of a helium ion that is trapped interstitially* and one of a helium ion that enters the film and leaves after a while, are given in fig. 29.

To study the effects of helium on deposited films, the following simulations have been calculated:

- A (100) PVD film with a 1.0 percent defect concentration and maximum cluster size of four has been decorated. The helium dose was $5*10^{14}/cm^2$, somewhat higher than the usual experimental dose of $1*10^{14}/cm^2$ or $2*10^{14}/cm^2$. In a separate simulation, the configuration in which two thirds of the $5*10^{14}/cm^2$ dose had been implanted has been annealed for 0.7 ns at 1500 K to study the mobility of helium in the lattice. During annealing atomic displacements of molybdenum were observed. In order to check which part of the displacements is due to the helium ions and which part would have taken place

* At a real experiment timescale, interstitial helium atoms are mobile at room temperature and are not considered to be trapped in interstitial positions.

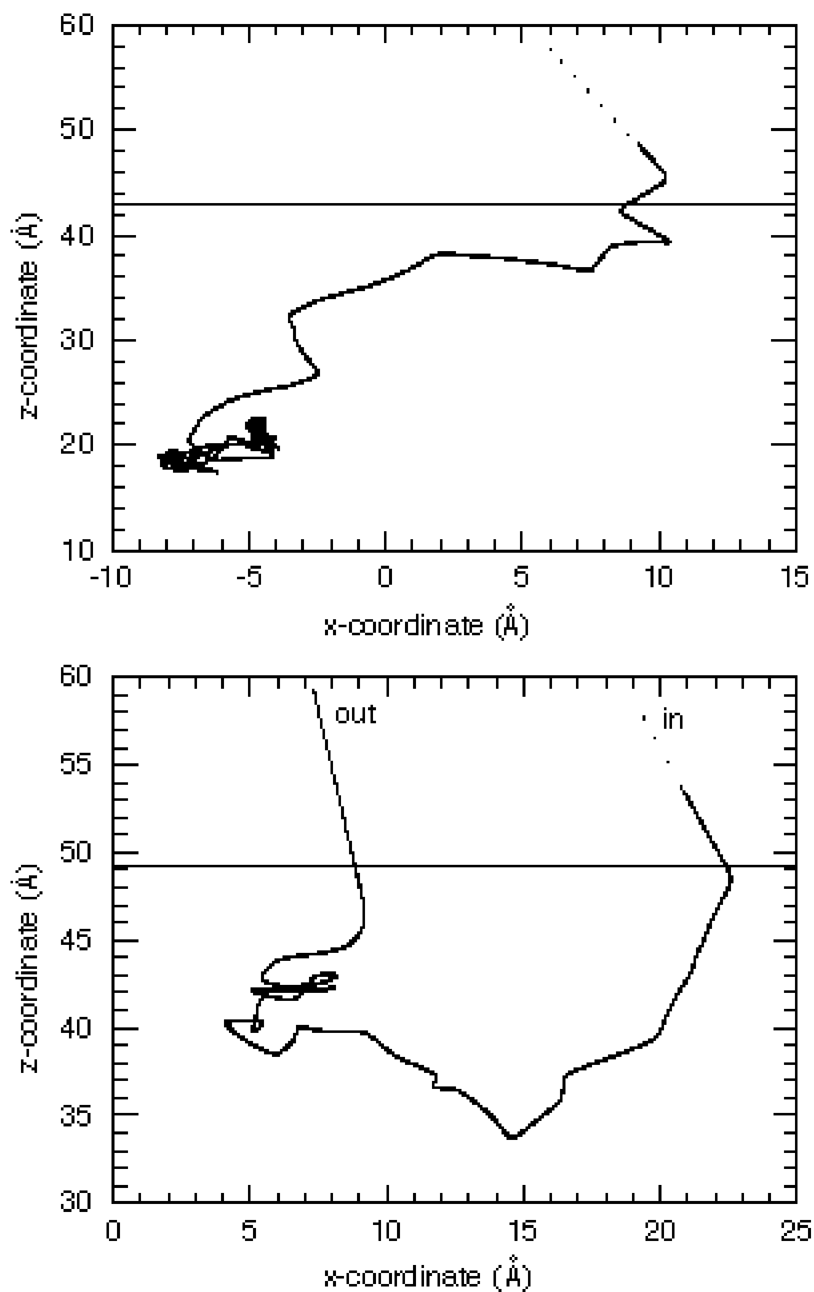

Figure 29. xz-projections of two helium trajectories. The upper figure is that of a helium ion that remains trapped in an interstitial position, the lower projection is that of a helium ion that collides through first 19 Å of the film and then leaves again. The vertical lines indicate the position of the surface at the point of impact.*

anyway in a simulation without helium, the original film without helium decoration has also been annealed for 0.7 ns at 1500 K.

---

* animations of a helium ion that traps and of a helium ion that leaves again after pentrating the surface can be viewed in the files hetrap.mov and heinandout.mov.

- A (100) IBAD film (100 eV with 10 percent 250 eV argon, IAR = 0.1) with four vacancies (vacancy concentration 0.1 %), six molybdenum self-interstitials, and three trapped argon ions has been decorated with a $5*10^{14}/cm^2$ helium dose and then annealed at 1500 K for 5 ns.
- A (110) IBAD film (100 eV with 10 percent 250 eV argon, IAR = 0.1) with a vacancy concentration of 0.2 percent without argon atoms has been decorated with a high helium dose, $2*10^{15}/cm^2$. The high dose was used to see if any trap mutation (a process in which a number of helium ions, trapped in the same vacancy, remove an adjoining molybdenum atom from its lattice position) would occur.
- A (110) IBAD film (25 eV argon with 10 percent 250 eV argon, IAR = 0.1) with a vacancy concentration of 0.6 percent and three trapped argon atoms has been decorated with a $5*10^{14}/cm^2$ helium dose.

All films contain a high number of helium ions after decoration, see table V.

Table V. Data for helium decoration runs. The number of helium ions in the bombardment, the number of backscattered helium ions, the number of helium ions trapped in interstitial sites, the number of helium ions trapped in vacancies or clusters, and the number of helium ions temporarily trapped between columns. The ions trapped between columns should be disregarded, because in a real experiment they would have had sufficient time to diffuse away from between the columns.

decorated film	# of helium ions in bombard-ment	fraction of helium ions backscattered during the simulation	fraction of interstitial trappings	vacancy concentra tion in film	fraction of trappings in vacancies or clusters	fraction of trappings between columns
(100) PVD	100	0.69	0.12	$1*10^{-2}$	0.19	0
(100) 100 eV IBAD	100	0.66	0.30	$1*10^{-3}$	0.04	0
(110) 25 eV IBAD	100	0.68	0.11	$6*10^{-3}$	0.21	0
(110) 100 eV IBAD	400	0.825	0.1125	$2*10^{-3}$	0.0425	0.02

Trapping at argon filled vacancies was never observed, probably because of the small number of argon atoms involved in the decoration runs. In all four simulations the fraction of backscattered helium ions is significantly higher than the fraction predicted by TRIM, which is 0.45.

The number of helium ions in the film does not show a clear relation to the defect concentration. However, in the films with high vacancy concentrations the fraction of helium ions trapped in vacancies is higher. In the films with low vacancy concentrations, most of the helium ions in interstitial positions would have diffused out of the film in a real experiment. In films with high vacancy concentrations part of the interstitial helium would have been trapped in vacancies. If only the helium ions trapped in vacancies are taken into account, there is a clear relation between the number of defects and the number of trapped helium ions. Figure 30 shows the trapping probabilities of the four decoration runs compared to HOP [18] calculations. It can be seen from fig. 30 that MD results and HOP results agree reasonably well.

The surface orientation has little influence on the amount of helium ions trapped in the films, the three films with a $5*10^{14}/cm^2$ dose all contained more or less equal numbers of helium ions. The film with the higher dose does not contain four times as many ions, but this is probably due to the very rough columnar structure, which always provides short escape routes from the lattice for helium ions. So depending on the deposition parameters some (110) films contain less helium after decoration.

When a helium atom moves close to a vacancy or cluster, closer than three atoms away from it, it often happens that the presence of the helium atom causes the molybdenum atom(s) between the helium atom and the vacancy/cluster to move one step closer to the vacancy/cluster, splitting off a vacancy from the cluster or moving the vacancy, see fig. 31.

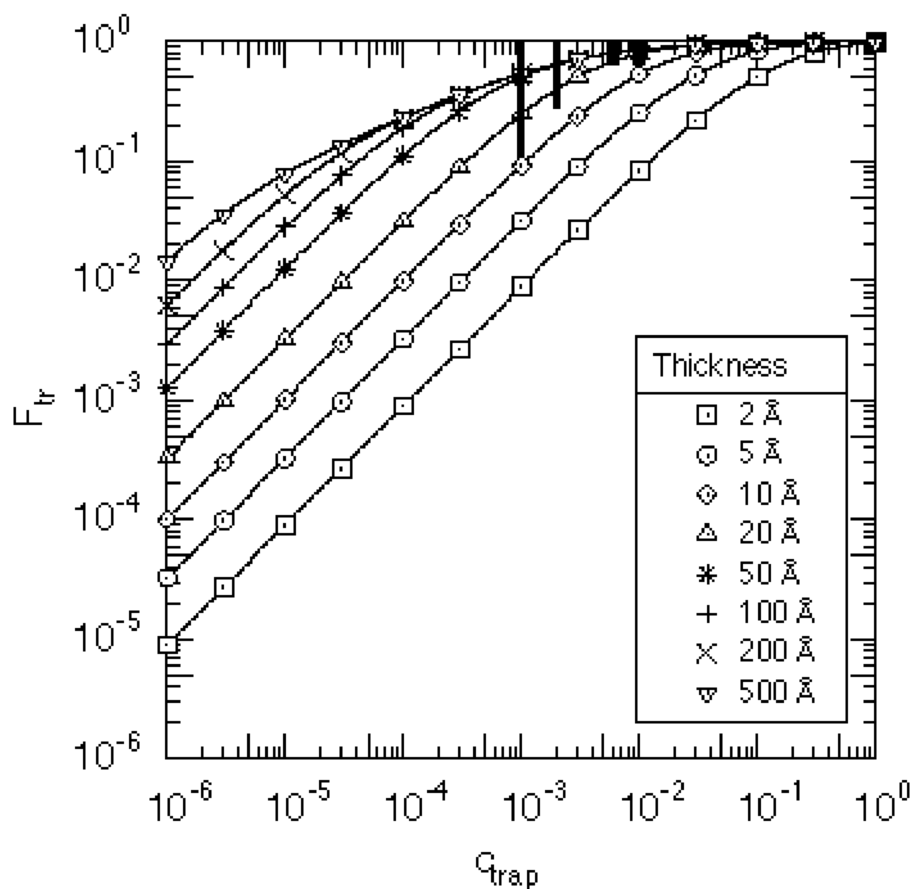

Figure 30. The helium trapping determined by MD simulations (black bars) compared to results calculated by HOP [18]. The low ends of the bars indicate the helium trapping if all helium atoms in interstitial positions were to desorb from the film. The high ends indicate the helium trapping if all helium atoms were to trap in vacancies. Note that HOP calculations are not MD calculations, HOP determines diffusion in the presence of vacancies.

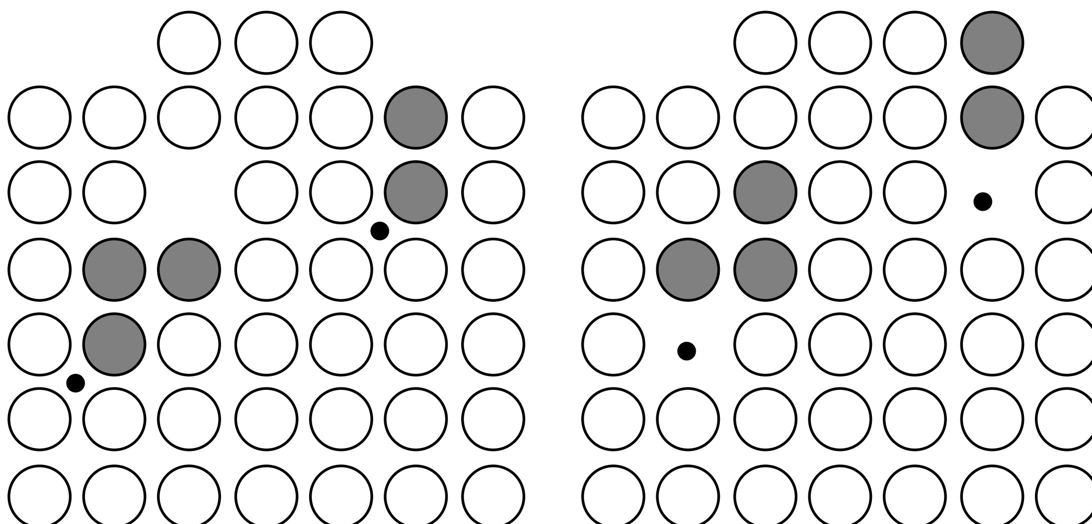

Figure 31. Vacancy displacement by a helium atom. When helium atoms (indicated by the small black circles) moves close to a vacancy or the surface, the molybdenum atoms between the helium and the vacancy or surface (indicated by the shaded circles) sometimes move one lattice step towards the vacancy or surface, effectively moving the vacancy (or unoccupied surface position) towards the helium.*

* An animation of this process can viewed in the file bivacancysplit.mov

So a helium atom tends to bias atomic displacements in a direction that attracts a vacancy to the helium ion. This phenomenon also takes place near the surface. In the film with only one vacancy all substitutional trappings took place by attracting vacancies from the surface. The driving force for moving the molybdenum atoms is mostly the stress the helium atom creates as an interstitial particle, not the kinetic energy with which it is injected into the film. This became clear when helium atoms also attracted vacancies during the annealing runs, when they only had thermal energy corresponding to 1500 K* . In the (100) PVD film six helium ions that initially were interstitials, became trapped in vacancies during annealing. Four of these were trapped by attracting a vacancy to an occupied lattice site, the other two moved into an existing vacancy or bivacancy. In the (100) 100 eV IBAD film three interstitial helium ions moved to monovacancy positions, one into the single vacancy present in the film, the other two by attracting vacancies from the surface.

Two-thirds of the molybdenum atomic displacement events near interstitial helium that took place in the decorated film did not take place when the same film was annealed before decoration. This shows that it is indeed the interstitial helium that causes the atomic displacement, and that it is not a matter of the helium atom moving into vacancies that just happened to move toward the helium atom. As far as we know, this mechanism has not been reported earlier.

Trap mutation was never observed. In films with many defects this is probably due to the fact that because of the high number of vacancies no one vacancy was ever filled with six or seven ions, the number needed to induce trap mutation [19]. Two helium atoms in a monovacancy was the maximum number observed in simulations. In films with few vacancies most helium ions were located in interstitial positions. Prolonged annealing of these films in future simulations could cause several helium atoms that do not desorb from the film to diffuse into the few existing vacancies present (or they could be placed there artificially), and this may eventually lead to trap mutation.

Helium desorption was never observed in either annealing run. Helium atoms in traps remained trapped and those in interstitial positions became trapped in existing vacancies or vacancy clusters or by attracting vacancies from the surface, from which they never desorbed during any simulation. This creation of defects near the surface could be the explanation of surface defects in TDS spectra: experimental TDS spectra [20] indicate the presence of surface defects in monocrystalline (110) films that lie within 5 Å from the surface. Helium desorbs from these defects between 400 and 700 K. Helium desorbs from bulk vacancies at 1200 K. There is convincing evidence that these defects are created by the 100 eV helium ions. Surface relaxation reaches deeper than 5 Å. Perhaps the different lattice spacing near the surface is the cause of different desorption temperatures for vacancies near the surface and in the bulk of the film. This would then explain the surfaces defects found in experiments. It would indicate that damage near the surface is not caused by the 100 eV impact (the time for any interaction is too short to cause defects), but by the stress in the lattice caused by thermalized helium. However, in the simulations helium ions attract vacancies from the surface in both (100) and (110) films. Experimental TDS spectra of (100) films show hardly any surface defects. A possible explanation lies in the rough film surface of simulated films. Simulated films do not contain large flat surfaces due to the high deposition rate. Perhaps the many lattice steps and other surface features of simulated (100) films enables helium ions to push out molybdenum atoms, whereas on real, flatter surfaces this may be impossible. This would explain why the experimental (100) spectra do not show surface defects.

A second disagreement between simulations and experiments is the number of surface defects compared to bulk defects. The (100) IBAD film has a defect concentration closest to experimental values. Almost all helium ions were trapped as interstitials in this film. Continued annealing of this film would trap most of the helium ions near the surface, because there are hardly any defects in the film to trap in and near the surface they would attract vacancies. This would indicate that in experimental spectra the number of surface defects should be far greater than the number of all other defects combined. This is not true.

---

* It is not known if this mechanism also works for interstitial argon atoms, because configurations with interstitial argon were never annealed.

An attempt to explain this could be made by pointing out that in reality interstitial helium ions leave the lattice at a low temperature instead of 1500 K, the temperature used in the simulation. At low temperature it is harder for helium ions to cause molybdenum displacements, because there is less thermal energy to assist in the process. This would explain the smaller number of surface defects in experiments.

The explanations above are based on a number of assumptions whose validity can not be proven on the basis of the available simulation data. Simulating helium decoration of perfectly flat (100) and (110) films followed by annealing could help to clarify the issue of the surface defects. For the moment the results from helium simulations must be regarded as having poor reliability. There is no explanation why results of helium simulations show so much less agreement than those of argon simulations (although argon desorption was never studied because it requires such high temperatures that it will never occur during a simulation), while the pair potentials for both are based on the same theory. A possible explanation for the behavior of helium near the surface (which is hard to verify experimentally by TDS) is an erroneous surface relaxation resulting from the simulations. The error may not lie in the molybdenum-helium interaction, but in molybdenum-molybdenum interactions near the surface.

4.5 Annealing films

To study the effects of annealing, but also, to gather information that would help to estimate what would happen if room temperature simulations would be possible at laboratory time scales, two films have been annealed at 2000 K. One was a (110) film with columnar structures and four monovacancies (vacancy concentration $1.3*10^{-3}$). It was annealed for 10 ns. The other was a (100) film with a large void and a total vacancy concentration of 3 percent, also annealed for 10 ns. Neither contained any argon or helium. A third film with (110) orientation, containing three vacancies, two argon ions, two self-interstitials, and a small dislocation loop (formed by clustering of self-interstitials), was annealed at 1500 K for 2 ns. Also, four bulk samples of molybdenum, each containing a number of monovacancies, were annealed at 500, 1000, 1500, and 2000 K. The first three were annealed for 0.7 ns, the fourth was annealed for 2 ns.

4.5.1 Surface diffusion

The most prominent annealing effect that was found for the surface is a decrease of the number of low-coordinated atoms on the surface. At the start of the simulation there are a number of atoms that ‘stick out’ and have five or fewer neighbours. During annealing at 2000 K, these atoms are found to be very mobile, even during the very short time of the simulation. They move over the surface, until they get trapped at more stable, higher-coordinated sites. In this way, the number of low-coordinated atoms decreases very rapidly. During the first two tenth of a ns the number of atoms with five or fewer neighbours decreases from 45 to 2 for the (110) film annealed at 2000 K. There are also atoms, however, that break free from high-coordinated sites and start moving over the surface. So the number of mobile atoms does not asymptotically decrease to zero, but to a certain value dependent on the annealing temperature. As an example, the (110) film before and after annealing at 2000 K is displayed in fig. 31. It can be seen from fig. 31 that the ‘macroscopic’ roughness has hardly changed at all.

Figure 32 shows the sum over all atoms of the distances by which atoms are displaced per annealing interval of 0.355 ns, excluding thermal vibrations, for the (100) film at 2000 K. It can be seen from figure 32, especially from the number of atoms participating in diffusion, that the diffusion has *almost* reached a constant level within 9 ns.

The decrease in the number of low-coordinated atoms and other relaxation effects

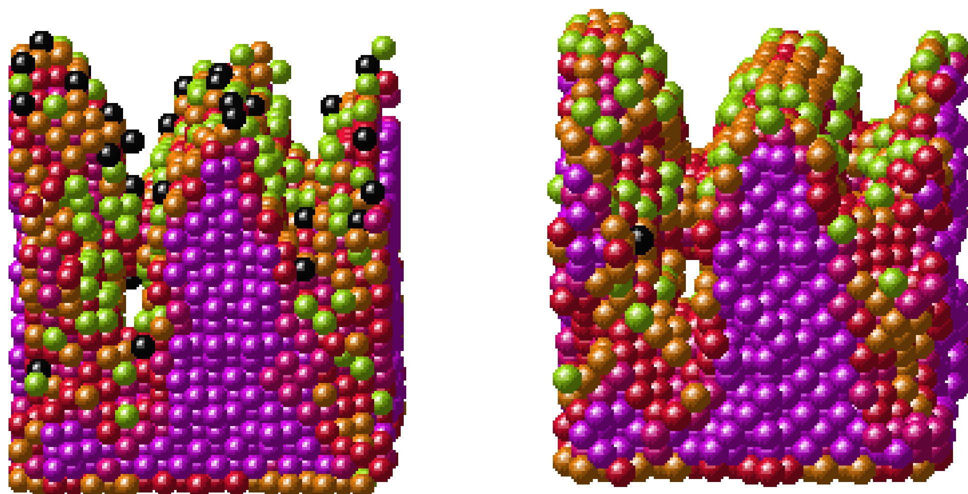

Figure 31. Top part of a columnar film on a (110) surface before (left) and after (right) annealing for 5 ns at 2000 K. The dark atoms are atoms with five or fewer neighbours.*

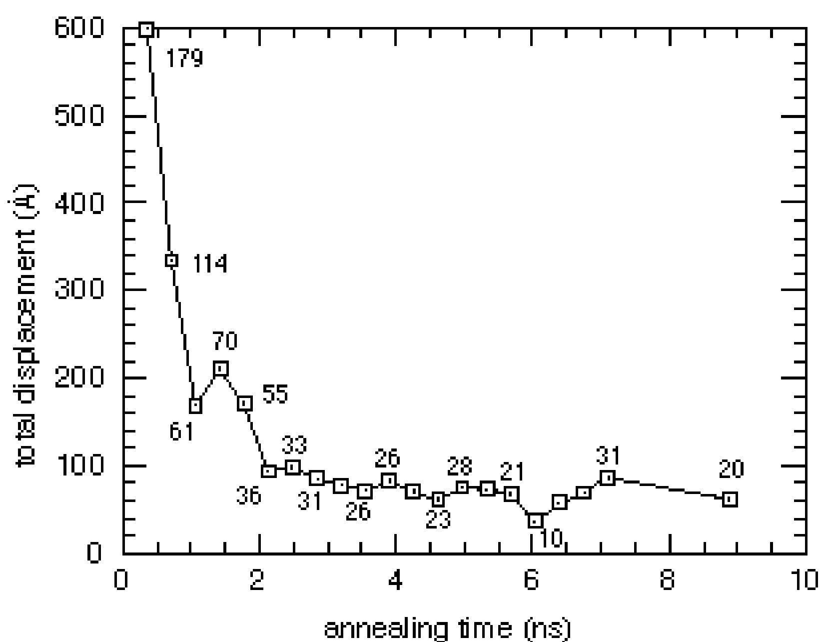

Figure 32. Sum over all atoms of the distances by which atoms have been displaced during the previous 0.355 ns time interval prior to the data point. Thermal vibrations have been excluded by cooling configurations to near 0 K prior to measuring the displacements. The figures near data points are the number of atoms responsible for the total displacement.

lowers the average potential energy during annealing. Fig. 33 shows the average potential energy as a function of annealing time for the (110) 2000 K film.

---

* An animation of the annealing process can be viewed in the file anneal.mov.

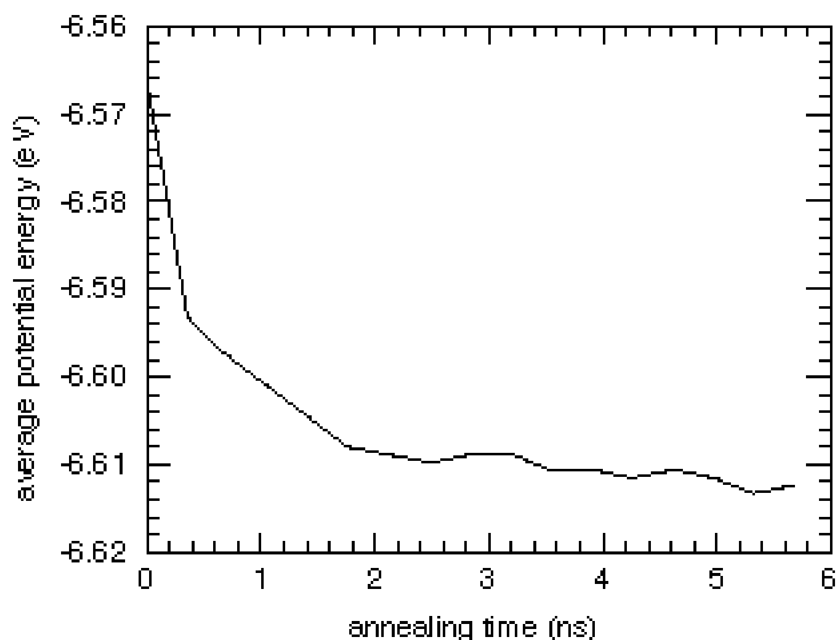

Figure 33. Potential energy per atom of a (110) film during annealing. Configurations have been cooled before measuring the potential energy.

Note the similarity between figs. 32 and 33. Both indicate that by extending the simulation for, say, another 8 ns, the film will not reach its expected lowest-energy shape, a flat surface with one lattice step. With current CPU power it is impossible to reach this stage.

What are the implications of the previous results for the existence of columnar structures? First it can be concluded that of all possible diffusion processes only diffusion requiring low activation energies is of any significance for the evolution of the surface. This is clear from the observation that at 2000 K practically all diffusion is caused by low-coordinated atoms, even while at 2000 K diffusion requiring higher activation energies is accelerated far more compared to room temperature (see also section 4.3.4) than diffusion requiring lower activation energies. So when comparing simulations with experimental results, only low-coordinated atoms need to be considered (they have low activation energies for migration), because only these could have moved in a real experiment. Figure 34 shows the number of atoms with five or fewer neighbours during the deposition of the first part of a (110) film under IBAD conditions similar to the (110) film that was annealed at 2000 K, together with the same data for a (110) PVD film deposited at 2000 K. From figure 34 it can be seen that during the deposition of the first 26 Å the number of low-coordinated atoms is more or less constant in the IBAD deposition run. After 26 Å the surface has roughened so much that the first columnar protrusions have appeared and that a further transition to columnar growth is already inevitable, see figure 35. This shows that the film surface evolves from a flat surface to a columnar structure without a change in the number of low-coordinated atoms. The PVD film shows an increase in the number of low-coordinated atoms between 5 and 15 Å of deposited film, but the increase is only about half the number of low-coordinated atoms present after 5 Å, and during the deposition of this part of the film the surface changes from almost flat to a surface with the early stages of columns and holes that will not be filled after continued deposition. So neither film shows a strong relation between the number of low-coordinated atoms and the formation of columns. From this is can be concluded that the appearance of columns is not strongly related to the behaviour of low-coordinated atoms and that the presence of columns in

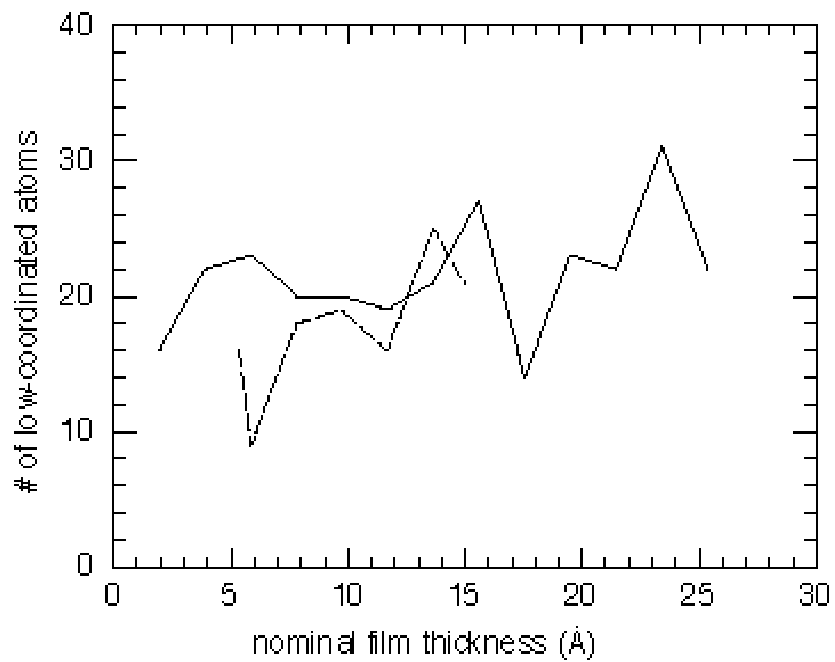

Figure 34. Number of atoms with five neighbours or less during IBAD deposition of a (110) film at 300 K (full curve) and deposition of a PVD film deposited at 2000 K (dashed curve).

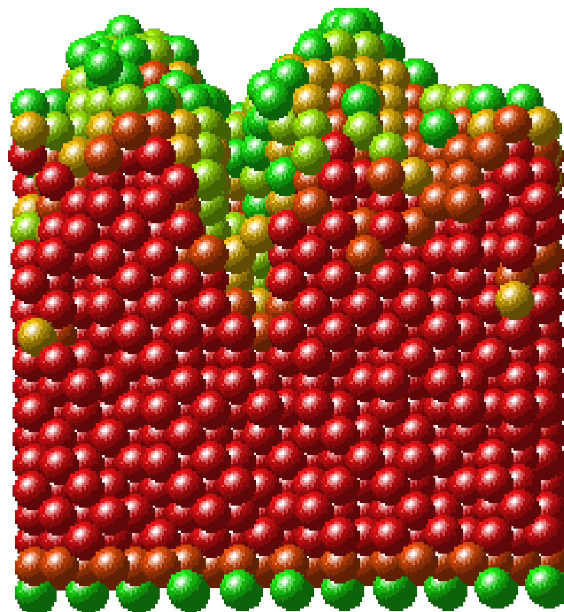

Figure 35. (110) IBAD film after 26 Å of nominal deposition. Colours indicate potential energy.

simulations is not, or only for a small part, the result of the high deposition rate, confirming the results of section 4.3.4.

4.5.2 Bulk diffusion

Clearly, the simulations that were calculated to study surface diffusion can also be used to study bulk diffusion. However, the (100) film annealed at 2000 K contained a high number of vacancy clusters. Once mobile, monovacancies tend to attach themselves to these clusters, which have proven to be immobile in the simulations. Therefore unhindered diffusion of monovacancies, which does take place in experiments, cannot be studied in the simulations. In the (110) film annealed at 2000 K almost all atoms are located near a surface because of the columns, and because of the surface relaxation not many atoms are left in representative 'bulk' positions. This is not a suitable situation to study monovacancy diffusion. The film annealed at 1500 K contained only three vacancies, two of which were immobilised because they contained argon atoms, and the third moved too little to lead to firm conclusions. In other films, too, the very small number of diffusion steps sometimes made it difficult to draw quantitative conclusions about bulk diffusion.

Since monovacancy diffusion is important in experiments and the previously mentioned simulations are unsuited to study monovacancy diffusion, four simulations were carried out solely to study monovacancy diffusion. The simulations were performed in boxes with periodic boundary conditions in all directions, which contained 8165 atoms and 27 monovacancies. Three boxes were annealed for 0.709 ns at 500, 1000, and 1500 K, the fourth box was annealed for 2 ns at 2000 K. It was found that in the films annealed at 500 and 1000 K not one vacancy ever moved, in the film annealed at 1500 K 17 vacancy jumps were observed, and in the film annealed at 2000 K the vacancies jumped so often that it was difficult to determine the vibrational frequency from this run[*]. Because of this, the activation energy had to be determined from just the simulation at 1500 K. The vibrational frequency is determined by counting the number of times an atom next to a vacancy moves closer to and further away from its equilibrium position. In determining the distance, only the projection on the line through the equilibrium positions of the atom and the vacancy is taken into account, because in the directions perpendicular to this direction, the frequency may differ from the frequency along the atom-vacancy line. The vibrational frequency of atoms next to a vacancy was determined as $6.2 * 10^{12}$ Hz. The number of attempted jumps per second per atom surrounding the vacancy is equal to the vibrational frequency, so in this case j in eqn. (31) equals 1. If all eight atoms surrounding the vacancy are considered as independent, the number of attempted jumps is eight times the vibrational frequency. If all eight atoms are considered as moving in one strongly coupled motion, the number of attempted jumps is equal to the vibrational frequency. Based on these extremes, the activation energy lies between 0.71 and 1.0 eV, a value lower than the value [21] of 1.3 eV found in simulations using the Johnson-Wilson potential. There is no clear explanation for this difference, except that the model (eqn. (31)) used in this thesis to interpret MD results is rather crude.

In the boxes that contained many vacancies and clusters most monovacancies attach to clusters after a few diffusion steps. Clusters of vacancies consisting not of nearest but next-nearest neighbours and elongated clusters tend to become more compact. Almost all clusters consist of vacancies in nearest-neighbour positions after annealing. These clusters are immobile for the duration of the simulation once they have formed.[*]

The main interest in the film with only three vacancies annealed at 1500 K is the mobility of self-interstitials. After annealing the film all isolated interstitials had disappeared. When comparing this to simulations involving helium it can be concluded that self-interstitials are much more mobile than helium interstitials at 1500 K: when films with interstitial helium are annealed at 2000 K, the helium atoms move no more than three or four positions every ns. The molybdenum interstitials all have disappeared in less than one ns at 1500 K, while the shortest route to the surface was 10 atomic planes long for one self-interstitials. This means that the creation of an interstitial plane is unlikely to occur in a real

---

[*] It is difficult to observe the behaviour of a vacancy because the atoms that surround the vacancy must be known before the simulation is started.

[*] A simulation of the annealing of a (100) surface with a large hole and other vacancies/clusters can be viewed in the file 1014.mcm

experiment, unless a very high number of interstitials is created in a very short time. Otherwise the interstitials diffuse away too fast for them to cluster into an interstitial plane. The small interstitial plane that had formed (probably the result of the high IBAD rate considering the previous remarks) proved quite stable. It did not disappear after annealing for 2 ns at 1500 K, nor did it seem to lose or gather any interstitials. This last conclusion should be handled with care, because determining the exact size of the interstitial plane proved quite difficult. The plane did not show any relaxation. This is probably because during deposition the ion bombardment had already introduced enough energy for the interstitial plane to take its most favourable position, or because to box size is too small.

5 Conclusions & recommendations

In order to study events during IBAD deposition and TDS at the atomic level, MD code has been written and potentials have been constructed to perform simulations. These simulations can provide very detailed information about all the atoms in system that is being studied. Despite the single precision numbers and complex algorithms used in the Camelion MD code, it works reliably. No unrealistic effects were detected from the adaptations to the Johnson-Oh EAM potential either. Only the surface relaxation results (and the results for helium close to surfaces) appear to be unreliable. However, many results for surface relaxation, both from experiments and simulations, are unreliable, so that there is no data that can prove the correctness or incorrectness of the simulation results in this thesis beyond doubt. In general the results produced by the program can be regarded as reliable as long as the physical reality of the simulated system does not suffer from the general simulation restrictions (lack of electronic heat conductance, small box size etc.).

The most important restriction for the simulations is the short simulation time, which enforces an extremely high deposition rate. The lack of any significant diffusion during the few nanoseconds of deposition results in an unrealistically high vacancy concentration when compared with real experiments, and an arguably too rough surface. Extending the simulation to laboratory time scale is not yet possible. However, deposition at elevated temperature can increase diffusion by orders of magnitude. Deposition at elevated temperature is therefore a simple way of determining at least the direction in which changes will take place if more diffusion is allowed. There is no danger that raising the temperature will cause processes to occur in the simulation that would not occur at room temperature, because at high temperature almost all diffusion is still caused by the same small fraction of low-coordinated atoms that cause diffusion at low temperature. Therefore performing more simulations at elevated temperatures is recommended. Another way of extending the simulation time scale would be using the Monte Carlo method. However, this method is very hard to implement for complex systems such as deposited films, because of the high number of activation energies.

Despite the limited diffusion, some interesting observations were made about the deposition of films. Most important are the mechanisms responsible for the inclusion of vacancies and vacancy clusters (reconnection of edges into a flat surface) on (100) surfaces and the growth of columns on (110) surfaces by protrusions that, rather than reconnect, attract more of the incoming atoms. The last observation explains the decrease in the number of vacancies with thickness in (110) films because unoccupied lattice sites are not sealed off, but are incorporated in the boundaries between columns. Another observation from deposition simulations is the clear influence of the deposition angle: a wave-like pattern on (110) surfaces and large holes on (100) surfaces. Unfortunately, the appearance of large holes is as yet unexplained by a simple mechanism.

The events following the impact of ions are short-time events and can therefore be studied in a simulation without having to distrust the results because of the short simulation time scale. This is a good example of the useful combination of experiments and simulations. Simulations with argon ions show the occurrence of replacement collision sequences, sputtering, the displacement of atoms and the number of displaced atoms, the trapping of argon ions and the mechanisms by which this trapping takes place etc. These events result in a decreased vacancy concentration compared to simulated PVD films, and a flattening of the surface. The short time events are difficult or impossible to study in experiments, but their influence can be verified through changes they cause in properties that can be measured experimentally. With the exception of the sputtering yield for (100) surfaces the results obtained for argon ions all agree well with experimental results. A further check of the reliability of the simulations could be made by determining the implantation profile of argon ions more accurately (an experimental argon implantation profile is available). A comparison of the implantation profile determined from simulations and experiments could also serve to check the reliability of the helium implantation profile that was determined from MD simulations. The influence of the argon ions on the surface roughness and the occurrence of RCSs can not be determined from TDS experiments, but both seem credible enough.

The helium simulations have yielded some interesting results as well. Simulations show that helium ions in molybdenum scatter after short lengths and an implantation profile was determined. Also, a mechanism was observed by which helium can attract vacancies and split vacancies from vacancy clusters. This mechanism, which as far as we know has thusfar not yet been reported, is also a possible explanation of the occurrence of defects near the surface found in experiments. However, the agreement between the results of the helium simulations and experiments or TRIM results is not as obvious as in the case of the argon simulations. The implantation profile determined from MD simulations is in disagreement with TRIM results. However, this is probably the result of the ignoring of backscattered ions that did penetrate the film by TRIM. On the other hand, other disagreements, such as the considerable number of helium ions trapped by attracting vacancies from the surface compared to the number of helium ions trapped in bulk vacancies, are not as easily explained. Experiments show no (for a (100) single crystal) or few (in some (110) single-crystal experiments) surface defects compared to bulk defects. The explanation that the vacancies in the simulation are formed as a result of the high film temperature during their formation, is only partly satisfactory. It does not explain why in simulations both (100) and (110) films have helium atoms trapped near the surface, while in experiments (100) films have hardly any helium atoms at all trapped near the surface. Although the trapping of helium near the surface is interesting as a possible explanation of the so-called surface peak in TDS spectra, further investigation using the same atomic interactions is of limited value, because the explanation of the apparent disagreement may not lie in the helium interactions, but in the Mo-Mo interactions near the surface. If that were indeed the case, more results obtained in this way may have to be re-calculated.

Three important conclusions can be drawn from the annealing of films and deposition of films at elevated temperatures. The first is that the presence of high numbers of vacancies and low-coordinated atoms are definitely the result of the high deposition rate. This is clear from the reduction of the number of low-coordinated atoms during the first stages of annealing and during deposition at 2000 K. The second conclusion is that only these low-coordinated atoms would participate in any significant diffusion if the simulation timescale was stretched by a factor of $5*10^9$ in order to be realistic. The third conclusion is that the disappearance of low-coordinated atoms during real deposition only results in a small reduction of the surface roughness and therefore the presence of columns is not (or only for a small part) the result of the high deposition speed. These conclusions are based purely on observations of low-coordinated atoms (atoms with low activation energies for migration) during ‘real’ diffusion, viz. how mobile these atoms are and where they find positions with deeper potential energy minima. Attempts to describe atomic motion during annealing or deposition in terms of a few activation energies have shown to be futile because there are hardly any atoms on any one surface that are in the same position in terms of activation energies. Due to surface relaxation and the large number of possible local surroundings, a spectrum of activation energies is required even on single crystals to describe diffusion.

Acknowledgements

The work I have done to produce this thesis I have done with pleasure. I would like to thank dr. Barend Thijsse and ir. Leon van Ee for the valuable discussions I have had with them, the ideas they proposed to me and all the answers to my many, many questions. Also, I would like to thank ir. Edwin Haddeman for his great linux-problem-solving skills and supernatural compiling talents which helped me out of the mess I sometimes managed to get myself into. My sincere gratitude to all three of you.

Peter Klaver

Literature

1 S. M. Foiles, MRS Bulletin, **21** (1996) p24-28
2J. Wang, A. Omeltchenko, R. J. Kalia, and P. Vashishta, Mat. Res. Soc. Symp. Proc., **455** (1997) p267-272
3H.M. Carlberg, E.P. Münger, and V. Chirita, Physical Review B, **54** p2217- 2224
4K. Morishita and T. Diaz de la Rubia, Mat. Res. Soc. Symp. Proc., **396** (1995) p39-44
5R. A. Johnson and D.J. Oh, J. Mater. Res., **4** (1989) p1195-1201
6W. Eckstein, *Computer Simulation of Ion-Solid Interactions* (Springer-Verlag, Heidelberg, 1991), p40.
7A. Robbemond, *Het maken van dunne films met behulp van ionenbundel-assitentie, bestudeerd met moleculaire dynamica.* (Masters Thesis, Delft University of Technology, Delft, 1996)
8H. Feil and H.J.W. Zandvliet, Phys. Rev. Lett., **69** (1992) p3076
9M. P. Allen and D.J. Tildesly, *Computer Simulation of Liquids* (Oxford Science Publications, New York, 1989), p78.
10J. van der Kuur, E.J. Melker, T. P. Huijgen, W.H.B. Hoondert, G.T.W.M. Bekking, A. van den Beukel and B. J. Thijsse, Mat. Res. Soc. Symp. Proc., **396** (1995) p587-592
11A. Robbemond and B.J. Thijsse, Nucl. Instr. and Meth. in Phys. Res. B, **127/128** (1997) p272-277
12 W. B. Zeper, *Computersimulatie van defekten in molybdeen m.b.v. de 'embedded atom'-mehtode*, (Masters Thesis, Delft University of Technology, Delft, 1986)
13 L. J. Clarke, Surface Science, **91** (1980) p131-152
14 B.A. Korevaar, M. Pols, J. van der Kuur and B.J. Thijsse, Nevacblad, **1** (1998), p3-10.
15 J. Bohdansky, J. Roth, and H.L. Bay, in J. Appl. Phys., **51** (1980) p2861-2865
16 N. I. Papanicolaou, G. A. Evangelakis, and G. C. Kallinteris, Computational Materials Science, **10** (1998) p105-100
17 J.P. Biersack and L.G. Haggmark, Nucl. Instr. Meth. **174** (1980) 257.
18 W. H. B. Hoondert,*Trapping and diffusion on noble gas atoms in some off-stoichiometric ceramics studied by thermal desorption spectrometry,* (Ph.D. Thesis, Delft University of Technology, Delft, 1993)
19 L. M. Caspers, R. H. J. Fastenau, A. van Veen, and W. F. W. M. van Heugten, Phys. Stat. Sol. (a) **46** (1978) p541-545
20 W. Buters, *Helium trapping in cold worked single crystalline molybdenum observed with thermal helium desorption spectrometry,* (Ph.D. Thesis, Delft University of Technology, Delft, 1987)
21 L.M. Caspers, A. van Veen, A. A. van Gorkum, A. van den Beukel, and C. M. van Baal, Phys. Stat. Sol. (a) **37** (1976) p371-383

Appendix A

This appendix contains the source code for the time step control algorithm.

```
C     *******
C     ** F **
C     *******
C     ** COMPUTE SIZE OF NEW TIMESTEP **

C       Execute first loop with (pre-set) zero timestep
      IF (STEP .EQ. 0) THEN
       GOTO 1015
      ENDIF

C       If timestep is fixed, skip further computations.
      IF (TIMALG .EQ. -1) THEN
       TIMADV = DT
       GOTO 1015
      ENDIF

C       ** The variable TIP is the running estimate of the **
C      ** timestep.                                 **

C       At the beginning of the first real time advance,
C       start with a rough estimate of the timestep.
      IF(STEP.EQ.1) THEN
        TIP = 0.0025
       TIP2 = TIP*TIP
      ENDIF

C       Debug: Count collision checks in free flight algorithm
      I01 = 0

C       Activate the next line to switch off the special free flight
c      algorithm
C      TIMALG = 0

      IF (TIMALG .GE. 0) THEN
C        Adaptive timestep control

       IF (TIMALG .EQ. 3) THEN
C          Initialization for the free flight algorithm.
              NFREE  = 0
         V2MXFR = 0.0
              DO I = 1, N
                     RLQUAB(I) = .TRUE.
              ENDDO
            ENDIF

       DO I = 1, N
         AA=VX(I)*VX(I)+VY(I)*VY(I)+VZ(I)*VZ(I)
         BB=VX(I)*AX(I)+VY(I)*AY(I)+VZ(I)*AZ(I)
         CC=0.25*(AX(I)*AX(I)+AY(I)*AY(I)+AZ(I)*AZ(I))

        IF (TIMALG .EQ. 3) THEN
C           Special preprocessor for the free flight algorithm.
C           Atoms are free (no net force), bound (net force),
C           or quasi-bound (free atoms just moved in close
C           to another atom but not yet experiencing a net
C          force).
               IF ((CC .NE. 0.0) .AND. QUASIB(I)) THEN
C            Remove quasi-bound status if atom experiences a
```

```
C              force.
            QUASIB(I) = .FALSE.
                 ENDIF
                  IF ((CC .EQ. 0.0) .AND. .NOT.QUASIB(I)) THEN
C              Atom is free, not bound or quasi-bound
                   NFREE = NFREE+1
                   IF (NFREE .GT. MAXFREE) THEN
                            WRITE(6,'("# free atoms= ",I18)') NFREE
                            WRITE(24,'("# free atoms= ",I18)') NFREE
                            WRITE(6,*) 'FATAL ERROR: ISFREE-ARRAY TOO SMALL'
                            WRITE(24,*) 'FATAL ERROR: ISFREE-ARRAY TOO SMALL'
                            CALL SPITOUT (1, STEP, TIME, 0, 0)
                   ENDIF
                   ISFREE(NFREE) = I
                          RLQUAB(I) = .FALSE.
C              Update max. square speed of free atoms
                          V2MXFR = MAX(V2MXFR,AA)
          ENDIF
                ENDIF

          IF ( (TIMALG. EQ. 0) .OR. ((TIMALG .EQ. 3) .AND.
    :                  RLQUAB(I)) ) THEN

C           This atom contributes to the timestep determination.
C           If the free flight algorithm is active, the atom is
C           bound or quasi-bound, otherwise it may be any atom.
C           NOTE: This IF-block has no indentation!

C           Atom without speed or acceleration cannot contribute
C           to timestep determination
          IF (AA.EQ.CC.AND.AA.EQ.0.0) THEN
           GOTO 1008
          ENDIF

          IF (BB.GE.CCA*SQRT(AA*4.0*CC)) THEN
C             If cosine of angle(v,a) is > -sqrt(8/9) the distance
C             traveled is a monotonuous function of time
           IF (I.EQ.1) THEN
C               For the first atom the current timestep may be too
C               large or too small
             VPHA2(I)=TIP2*(AA+BB*TIP+CC*TIP2)
1001           IF (VPHA2(I).GT.L2) THEN
C                Select next smaller timestep
              TIP = TIP*RFR
              TIP2 = TIP*TIP
              VPHA2(I)=TIP2*(AA+BB*TIP+CC*TIP2)
              GOTO 1001
            ELSE
1002             IF(VPHA2(I).LE.L2) THEN
C                 Try next larger timestep
               TIP = TIP/RFR
               TIP2 = TIP*TIP
               VPHA2(I)=TIP2*(AA+BB*TIP+CC*TIP2)
               GOTO 1002
             ENDIF
C              Timestep is one too large
            TIP = TIP*RFR
            TIP2 = TIP*TIP
            ENDIF
          ELSE
C              All subsequent atoms may only reduce the timestep
1003           VPHA2(I)=TIP2*(AA+BB*TIP+CC*TIP2)
            IF (VPHA2(I).GT.L2) THEN
```

```
           TIP = TIP*RFR
           TIP2 = TIP*TIP
           GOTO 1003
          ENDIF
         ENDIF

        ELSE
C          If cosine of angle(v,a) is < -sqrt(8/9) the distance
C          traveled is no longer a monotonuous function of time:
C          The atom may be on its way 'to make a turn'
         COSVA = BB/SQRT(AA*4.0*CC)
         A01 = SQRT(AA/(4.0*CC))
              A02 = 3.0*COSVA/2.0
              A03 = SQRT((9.0*COSVA*COSVA/4.0)-2.0)
C          TE is the time to the local maximum in the distance
C          traveled (i.e. the turning point).
C          This maximum distance is A04.
         TE = A01*(-A02-A03)
         TE2 = TE*TE
         A04 = TE2*(AA+BB*TE+CC*TE2)
C          TT is the time to the local minimum in the distance
C          traveled (i.e. on its way back). TT is larger than TE.
         TT = A01*(-A02+A03)
         IF (A04.LT.L2) THEN
C            L2 is so large that the atom will first make a turn
C            and then travel far backwards. This is not allowed.
C            The atom may not travel further back than roughly the
C            same distance from the turning point as where it came
C            from, and thus the timestep may not be larger than TT.
          IF (I.EQ.1) THEN
           TIP = TT
           TIP2 = TIP*TIP
          ELSE
           IF (TIP.GT.TT) THEN
            TIP = TT
            TIP2 = TIP*TIP
           ENDIF
          ENDIF
         ELSE
C            L2 is less than the distance^2 to the turning point,
C            so the atom must stop before the turning point. But
C            there may be two more points after the turning point
C            that have the same distance to the initial position.
C            These two should not be selected.
          IF (TIP.GE.TE) THEN
C             Current trial timestep is larger than TE.
C             Not allowed. Set to TE and reduce until safe.
           TIP = TE
           TIP2 = TIP*TIP
           VPHA2(I)=TIP2*(AA+BB*TIP+CC*TIP2)
1004          IF (VPHA2(I).GT.L2) THEN
C              Select next smaller timestep
            TIP = TIP*RFR
            TIP2 = TIP*TIP
            VPHA2(I)=TIP2*(AA+BB*TIP+CC*TIP2)
            GOTO 1004
           ENDIF
          ELSE
C             Current trial timestep is smaller than TE.
           IF (I.EQ.1) THEN
C              For the first atom the current timestep may be too
C              large or too small
            VPHA2(I)=TIP2*(AA+BB*TIP+CC*TIP2)
```

```
1005          IF (VPHA2(I).GT.L2) THEN
C              Select next smaller timestep
             TIP = TIP*RFR
             TIP2 = TIP*TIP
             VPHA2(I)=TIP2*(AA+BB*TIP+CC*TIP2)
             GOTO 1005
            ELSE
1006          IF(VPHA2(I).LE.L2) THEN
C              Try next larger timestep
              TIP = TIP/RFR
              TIP2 = TIP*TIP
              VPHA2(I)=TIP2*(AA+BB*TIP+CC*TIP2)
              GOTO 1006
             ENDIF
C             Timestep is one too large
            TIP = TIP*RFR
            TIP2 = TIP*TIP
            ENDIF
           ELSE
C             All subsequent atoms may only reduce the
C             timestep
1007          VPHA2(I)=TIP2*(AA+BB*TIP+CC*TIP2)
            IF (VPHA2(I).GT.L2) THEN
             TIP = TIP*RFR
             TIP2 = TIP*TIP
             GOTO 1007
            ENDIF
           ENDIF
          ENDIF
         ENDIF
        ENDIF
1008     CONTINUE
C        End of atom-contributes-to-TIMADV
        ENDIF
C        Next atom for TIMADV determination
       ENDDO

       TIMADV = TIP

C      **  WE NOW HAVE A TIMESTEP BASED ON THE VELOCITY  **
C      **  AND ACCELERATION OF (QUASI-) BOUND ATOMS.     **
C      **   NO SUCH ATOM TRAVELS FURTHER THAN L1 AWAY   **
C      **  FROM ITS STARTING POINT AT ANY POINT OF ITS   **
C      **  PARABOLIC TRAJECTORY IN TIME TIMADV.          **

C      Free         atoms, however, may travel further than L1. This
C       will only lead to disaster (i.e. a collision) if other
C       atoms come in their way. This has to be checked, and
C       TIMADV ahs to be reduced if there are impending
C       collisions. Note that a free atom may proceed safely
C       until the radius of influence of a (quasi-) bound atom
C      AT ITS POINT OF DEPARTURE, in view of the remark made
C       above.

       IF ((TIMALG .EQ. 3) .AND. (NFREE .GT. 0)) THEN
             IF (NFREE .NE. PNFREE) THEN
               WRITE(6,*) NFREE, ' free atom(s).'
             ENDIF
             VPHA2FRMX = V2MXFR*TIMADV*TIMADV
             IF (VPHA2FRMX.GT.L2) THEN
C          At least one free atom travels more than L1.
C          We need to check threatening collisions.
               COLLDET=.FALSE.
```

```
        DO II = 1, NFREE
      I = ISFREE(II)
      AA=VX(I)*VX(I)+VY(I)*VY(I)+VZ(I)*VZ(I)
      A01=AA*TIMADV*TIMADV
            IF (A01.LE.L2) THEN
C           This free atom travels no more than L1.
             GOTO 1010
            ENDIF
            DO J = 1, N
             IF (J .EQ. I) GOTO 1011

C           For (quasi-) bound atoms J the collision time
C           is to the point of departure of J (see above, why),
C           so we pretend that it doesn't move at all.
C           For free atoms J the collision time is
C           the real thing.
C           Note: The z direction is not periodic

        RZIJ = RZ(I) - RZ(J)
              IF (.NOT.RLQUAB(J)) THEN
               A03 = VZ(I) - VZ(J)
               A09 = RZIJ + TIMADV*A03
              ELSE
               A03 = VZ(I)
               A09 = RZIJ
              ENDIF
C           A09 is zi-zj at TIMADV

C  A09 = RZIJ + TIMADV*(A03-0.5*AZ(J)*TIMADV)
C  A05 is time to extremum in zi(t)-zj(t) vs. t
C  A08 is zi(t(extr))-zj(t(extr))
C        A05 = TIMADV
C        A08 = A09
C        IF (AZ(J) .NE. 0.0D0) THEN
C   zi-zj parabolic
C         A05 = A03/AZ(J)
C         IF (A05.LE.0.0 .OR. A05.GT.TIMADV) THEN
C              A05 = TIMADV
C         ELSE
C          A08 = RZIJ + A05*(A03-0.5*AZ(J)*A05)
C         ENDIF
C        ENDIF

C            A11 is the radius of influence of the I,J pair
              A11 = RCMAX(TP(I),TP(J))

C            Under certain conditions I and J cannot possibly
C            collide, so we don't have to check those pairs.
              IF (
   :       (RZIJ.GT. A11.AND.A09.GT. A11)
   :       .OR.
   :       (RZIJ.LE.-A11.AND.A09.LE.-A11)
   :       ) GOTO 1009

C                   We don't exclude any more pairs on simple grounds.
C            Now were we have to check the impending
C            collision time the hard way.
               RXIJ = RX(I) - RX(J)
         RXIJ = RXIJ - PERTBOXX*ANINT(RXIJ*BOXXI)
         RYIJ = RY(I) - RY(J)
         RYIJ = RYIJ - PERTBOXY*ANINT(RYIJ*BOXYI)
               IF (.NOT.RLQUAB(J)) THEN
                A01  = VX(I) - VX(J)
```

```
                    A02  = VY(I) - VY(J)
                   ELSE
                        A01  = VX(I)
                        A02  = VY(I)
                   ENDIF
                    A10  = RXIJ*A01 + RYIJ*A02 + RZIJ*A03

C                Time to collision between I and J
                    IF (A10 .LT. 0.0) THEN
C Debug
                     I01 = I01+1
C -1-
                        A04   =  A01*A01  +  A02*A02  +  A03*A03
                        A12 = A10*A10 - A04*(RIJSQ-A11*A11)
                        IF ((A12 .GT. 0.0) .AND. (A04 .NE. 0.0)) THEN
                         A05 = (-A10-SQRT(A12))/A04
                         IF (A05 .LT. TIMADV) THEN
                          TIMADV = A05

C  If a collision was detected in one of the steps before, then
C  restore the QUASIB-values of the collision partners.
                          IF(COLLDET) THEN
                           QUASIB(INDI)=IQUASIB
                           QUASIB(INDJ)=JQUASIB
                          ELSE
                           COLLDET=.TRUE.
                          ENDIF
C  Store QUASIB-values of collision pair I,J
                          INDI=I
                          INDJ=J
                          IQUASIB=QUASIB(I)
                          JQUASIB=QUASIB(J)

                          OPEN  ( UNIT = 17, FILE = INSFILE,
    :               ACCESS = 'APPEND', STATUS = 'UNKNOWN')
                    WRITE (17,
     : '(I7,I5,I4,F14.4,6(F9.4),'' Time to collision= '',F8.5)') STEP,
    :                ID(I), TP(I), TIME, RX(I), RY(I), RZ(I),
    :                VX(I), VY(I), VZ(I), A05
C    :                 RLQUAB(I),           QUASIB(I)
                    WRITE (17,
     : '(I7,I5,I4,F14.4,6(F9.4),'' Time to collision= '',F8.5)') STEP,
    :                ID(J), TP(J), TIME, RX(J), RY(J), RZ(J),
    :                VX(J), VY(J), VZ(J), A05
C    :                 RLQUAB(J),           QUASIB(J)
                   CLOSE ( UNIT = 17 )
C                    This pair has reduced the timestep.
C                    Mark both atoms as quasi-bound.
                          QUASIB(I) = .TRUE.
                          IF (.NOT.RLQUAB(J)) QUASIB(J) = .TRUE.
                         ENDIF
                     ENDIF
                   ENDIF
1009             CONTINUE
C                End of check pair for collision
1011          CONTINUE
C               Next partner J of free atom I
               ENDDO
1010          CONTINUE
C             Next free atom      I
              ENDDO
             ENDIF
       ENDIF
```

```
      PNFREE=NFREE
C Debug
      IF (TIMALG .EQ. 3 .AND. I01.NE.0) THEN
        WRITE(6,'("# collisions computed is ",I10)') I01
           ENDIF

C         End of adaptive timestep control
      ENDIF

1015  CONTINUE
```